

This item is the archived peer-reviewed author-version of:

The antioxidative role of cytoglobin in podocytes : implications for a role in chronic kidney disease

Reference:

Randi Elisa B., Vervaeke Benjamin, Tsachaki Maria, Porto Elena, Vermeylen Stijn, Lindenmeyer Maja T., Le Thi Thanh Thuy, Cohen Clemens D., Devuyt Olivier, Kistler Andreas D.,- The antioxidative role of cytoglobin in podocytes : implications for a role in chronic kidney disease
Antioxidants and redox signaling - ISSN 1523-0864 - 32:16(2020), p. 1155-1171
Full text (Publisher's DOI): <https://doi.org/10.1089/ARS.2019.7868>
To cite this reference: <https://hdl.handle.net/10067/1665030151162165141>

Forum Original Research Communication

The anti-oxidative role of cytoglobin in podocytes: implications for a role in chronic kidney disease.

Elisa B. Randi^{1,2,3}, Benjamin Vervaet⁴, Maria Tsachaki^{3,5}, Elena Porto⁶, Stijn Vermeyleen⁴, Maja T. Lindenmeyer^{2,3,7}, Le Thi Thanh Thuy⁸, Clemens D. Cohen^{2,3,7}, Olivier Devuyst^{2,3}, Andreas D. Kistler⁹, Csaba Szabo¹⁰, Norifumi Kawada⁸, Thomas Hankeln⁶, Alex Odermatt^{3,5}, Sylvia Dewilde⁴, Roland H. Wenger^{2,3}, David Hoogewijs^{1,3,*}

¹Department of Medicine/Physiology, University of Fribourg, Switzerland

²Institute of Physiology and Zurich Center for Integrative Human Physiology (ZIHP), University of Zurich, Switzerland

³National Center of Competence in Research (NCCR) "Kidney.CH", Switzerland

⁴Department of Biomedical Sciences, University of Antwerp, Belgium

⁵Division of Molecular and Systems Toxicology, Department of Pharmaceutical Sciences, University of Basel, Switzerland

⁶Institute of Organismal and Molecular Evolutionary Biology, University of Mainz, Germany

⁷Nephrological Center, Medical Clinic and Policlinic IV, University of Munich, Munich, Germany

⁸Department of Hepatology, Graduate School of Medicine, Osaka City University, Osaka, Japan

⁹Division of Nephrology, Kantonsspital Frauenfeld, Switzerland

¹⁰Chair of Pharmacology, Faculty of Science and Medicine, University of Fribourg, Switzerland

Running title: CYGB is implicated in CKD

Keywords: oxidative stress, reactive oxygen species, globin, diabetic nephropathy

* **Corresponding author:** e-mail: david.hoogewijs@unifr.ch, Tel: +41 26 300 94 10

Word count: 7578

Reference number: 75

Number of grayscale illustrations: 3 (+8 Supplementary)

Number of color illustrations: 3

ABSTRACT

Aims: Cytoglobin (CYGB) is a member of the mammalian globin family of respiratory proteins. Despite extensive research efforts, its physiological role remains largely unknown, but potential functions include reactive oxygen species (ROS) detoxification and signaling. Accumulating evidence suggests that ROS play a crucial role in podocyte detachment and apoptosis during diabetic kidney disease. This study aimed to explore the potential anti-oxidative renal role of CYGB both *in vivo* and *in vitro*.

Results: Using a *Cygb*-deficient mouse model we demonstrate a *Cygb*-dependent reduction in renal function, coinciding with a reduced number of podocytes. To specifically assess the putative anti-oxidative function of CYGB in podocytes, we first confirmed high endogenous CYGB expression levels in two human podocyte cell lines and subsequently generated shRNA-mediated stable CYGB knockdown podocyte models. CYGB-deficient podocytes displayed increased cell death and accumulation of ROS as assessed by H₂-DCF-DA assays and the redox sensitive probe roGFP2-Orp1. CYGB-deficient cells also exhibited an impaired cellular bioenergetic status. Consistently, analysis of the CYGB-dependent transcriptome identified dysregulation of multiple genes involved in redox balance, apoptosis as well as in chronic kidney disease. Finally, genome-wide association studies and expression studies in nephropathy biopsies indicate an association of CYGB with chronic kidney disease.

Innovation: This study demonstrates a podocyte-related renal role of *Cygb*, confirms abundant CYGB expression in human podocyte cell lines and describes for the first time an association between CYGB and chronic kidney disease.

Conclusion: Our results provide evidence for an anti-oxidative role of CYGB in podocytes.

INTRODUCTION

Cytoglobin (Cygb) belongs to the family of mammalian globins in addition to hemoglobin (Hb), myoglobin (Mb), neuroglobin (Ngb) and the recently identified androglobin (Adgb) (6). Most known globins fulfil respiratory functions, supplying the cell with adequate amounts of O₂ for aerobic energy production via the respiratory chain in the mitochondria (72). In contrast to Mb and Hb, the more recently identified globins Cygb (5,7), Ngb (5,7), as well as Adgb (27) all display hexacoordination of the heme iron atom (i.e. bound by two amino acid residues of the globin fold). While no functional interpretation for this heme hexacoordination currently exists, it is thought to point at a role other than the classical oxygen delivery and supply of Hb and Mb. The tissue expression profile of mammalian Cygb has been extensively studied (25). Cygb is predominantly expressed in fibroblasts and related cell types, but also in distinct nerve cell populations. Its physiological function, however, remains unclear; potentially, Cygb may have a role in oxygen storage, NO metabolism, ROS protection or signalling.

Several animal model studies assessed the functional role of Cygb. Singh and colleagues (60) suggested a major role of Cygb in muscle repair and regeneration as myogenic progenitor cells derived from a mouse model, in which Cygb was specifically knocked out in skeletal muscle, were severely deficient in their ability to form myotubes. Moreover, Thuy et al. (65) support the antioxidant role of Cygb using a global knock-out mouse model which displays age-dependent development of multiple organ abnormalities. Using the same Cygb-deficient model Liu et al. (36) recently provided evidence for a role of Cygb as regulator of NO degradation and cardiovascular tone in the vascular wall, in line with their previous *in vitro* observations on the NO dioxygenase function of Cygb (37). Additionally, Thuy et al. (66) and Yassin et al. (75) both reported an implication of Cygb in tumorigenesis using *in vivo* models.

The renal role of Cygb has been underexplored. Nakatani et al. (48) detected expression of Cygb in rat kidney, mainly in fibroblasts, but also in the glomerulus. Upon cyclosporine A induced nephropathy *Cygb* expression was upregulated in fibrotic lesions of the kidney, specifically in interstitial fibroblasts positive for renal fibroblast markers CD73 and α SMA. Thuy et al. (65) also observed substantially increased fibrosis in Cygb KO mice, mostly in

the liver, but also in the kidney, suggesting an antifibrotic role of Cygb. Similarly, Mimura et al. (42) and Nishi et al. (49) employed Cygb-overexpressing transgenic rats in disease models of remnant kidney and renal ischemia/reperfusion, respectively, to provide evidence for an antifibrotic role of Cygb in kidney fibroblasts, potentially via a ROS scavenging function. Despite these investigations the pathophysiological role of Cygb in the kidney, particularly in cell types other than interstitial fibroblasts, remains poorly understood.

Glomerular visceral epithelial cells, namely podocytes, are highly specialized cells in the Bowman's capsule of the kidney that actively participate in the glomerular filtration process due to their foot processes and slit diaphragm. Podocyte injury is the primary cause of impaired glomerular filtration. Accumulating evidence exists that oxidative stress plays a key role in most pathogenic pathways leading to podocyte defects, e.g. observed in diabetic nephropathy (19). Free radicals such as superoxide can induce cell and tissue injuries through lipid peroxidation, activation of NF- κ B (23), production of peroxynitrite and induction of apoptosis. Furthermore, ROS and other free radicals can directly induce cell injury. *In vitro* studies indicated that Cygb is able to scavenge free radicals, and overexpression of Cygb in renal immortalized fibroblasts (42,49) as well as in various other cellular models preserves cell viability under conditions of oxidative stress (12,26,33,61,74), but the role of Cygb in podocytes remains unexplored.

In the current study we employed a Cygb KO model to investigate the renal function of Cygb and observed a podocyte-associated phenotype. Using cellular models of human podocytes for mechanistic studies we demonstrated abundant CYGB expression in podocytes and investigated the anti-oxidative role of CYGB in human podocyte cell lines. Podocytes lacking CYGB displayed increased ROS accumulation and cell death, as well as altered expression of genes involved in the antioxidant defense system and apoptosis. Moreover, human renal biopsy expression data from chronic kidney disease (CKD) patients indicated an association of CYGB and advanced stage renal disease.

RESULTS

Cygb-deficient mice display reduced kidney function and reduced podocyte number

To analyze the renal expression pattern of *Cygb* we performed immunofluorescence analysis on mouse kidney tissue. Immunofluorescence revealed that *Cygb* is expressed in interstitial fibroblasts as well as in the glomerulus (Fig. 1A). To assess a potential *Cygb*-dependent effect on kidney function we employed a previously established *Cygb* KO mouse model (64). Reduced *Cygb* expression in *Cygb*^{-/-} mice was confirmed in whole kidney mRNA and protein extracts (Figs. 1B-C) as well as on immunofluorescence level (Fig. 1A). As compared to wild type mice, *Cygb*^{-/-} mice demonstrated a substantial reduction in renal function, as indicated by an increased serum FITC-sinistrin concentration and decreased clearance (Fig. 1D). However, analysis of plasma and urine electrolytes did not show significant differences between the two groups (Supplementary Fig. S1A-B). We also did not observe changes in marker genes of fibrosis and vasculature in whole kidney RNA (Supplemental Fig S6A). As we detected *Cygb* expression in the glomerulus we next investigated a potential role of podocytes in this phenotype. The average number of podocytes per glomerular cross section was determined by counting cells stained with the podocyte-specific marker Wt-1 (20). Although no apparent difference in proteinuria (Supplementary Fig. S1F) nor clear gross morphological kidney changes were observed in the two groups (Supplementary Fig. S1G), podocyte numbers were significantly reduced in *Cygb*^{-/-} mice compared to *Cygb*^{+/+} mice, as assessed by immunohistochemistry (Fig. 1E). Consistent with this observation, Wt-1 mRNA (Fig. 1F) as well as protein levels (Fig. 1G) were downregulated in *Cygb*^{-/-} mice, confirming a decreased podocyte number.

Abundant CYGB expression in podocyte cell models

To mechanistically investigate the role of CYGB in the glomerulus we explored CYGB levels in human podocyte cell culture models. Compared to various human kidney-derived cell lines, including proximal tubule cells, fibroblasts, embryonic cells most abundant endogenous CYGB mRNA and protein levels were observed in podocytes, particularly in AB8/13 (Fig. 2A), which was employed for subsequent investigations. The heat-sensitive AB8/13 cells proliferate at the permissive temperature of 33°C and stop proliferating and

undergo differentiation within two weeks at the non-permissive temperature 37°C (57). RT-qPCR revealed that CYGB mRNA is differently expressed before and after podocyte differentiation (Fig. 2B) and the CYGB protein is localized in both cytoplasm and nucleus, as assessed by immunoblotting (Fig. 2C).

We established stable AB8/13 knock-down cells using two independent shRNA sequences targeting CYGB, termed shCYGB-1 and shCYGB-2. CYGB knock-down efficiency was confirmed on mRNA and protein level (Figs. 2D-E). To obtain an independent podocyte cell culture model we also generated stably CYGB depleted shRNA LY cells (Supplementary Fig. S2).

Anti-apoptotic role of CYGB in AB8/13

A putative anti-apoptotic role of CYGB has been suggested in some cell lines (60,67), but not in podocytes. This prompted us to investigate cell viability in our cell models. CYGB knock-down podocyte cell lines displayed increased cell death (Fig. 3A), indicating a role of CYGB in cell survival. A similar reduction in cell viability was observed in the independently analyzed LY podocyte cell line (Supplementary Fig. S2). Consistently, we observed substantially increased cleaved-PARP1 levels in shCYGB-1 cells (Fig. 3B), but not in shCYGB-2, possibly due to its more moderate knock-down of CYGB. Moreover, MTT assays demonstrated that shCYGB-1 cells were more susceptible to H₂O₂ and AMA compared to WT and shCTR cells (data not shown). TUNEL assays revealed DNA double-strand breaks in shCYGB-1 and shCYGB-2 cells treated with H₂O₂ for 3 h, but not in shCTR cells (Fig. 3C).

Due to the intimate link between cell death and mitochondrial functions (ATP production and apoptosis), we investigated a potential CYGB-dependent effect on the bioenergetics status in AB8/13 cells. For this purpose, we analyzed mitochondrial respiration, measured as oxygen consumption rate (OCR). Cells were treated sequentially with oligomycin, FCCP and rotenone/AMA in order to challenge the mitochondrial electron transport chain and evaluate possible differences in OCR response. CYGB downregulation was associated with decreased OCR already at base line and also following addition of the various mitochondrial stressors (Fig. 3D). The lower OCR after oligomycin in shCYGB-1 cells is linked to lower ATP production compared to shCTR, consistent with a decreased mitochondrial activity. Subsequent FCCP treatment resulted in an increased maximal OCR in shCTR cells compared to CYGB knock-down cells. Until this stage, shCYGB-2 cells

(characterized by a less pronounced knock-down of CYGB than shCYGB-1 cells, Fig. 2E) displayed an intermediate phenotype between shCTR and shCYGB-1. However, after the final treatment with rotenone and AMA, shCYGB-1 and -2 cells reached the same minimal OCR, while shCTR cells displayed higher levels, suggesting a higher non-mitochondrial respiration in control cells compared to CYGB knock-down podocytes (Fig. 3E). Overall, these data indicate that CYGB supports podocyte viability by preserving mitochondrial bioenergetics.

Antioxidative role of CYGB in AB8/13

To further investigate the putative anti-oxidative role of CYGB in podocytes, we analyzed expression levels of the redox-sensitive genes *HO-1* and *HSP1A1*. Basal mRNA levels of both *HO-1* and *HSP1A1* were increased in shCYGB-1 cells compared to WT and shCTR cells (Supplementary Fig. S3), indicating a CYGB-dependent altered intracellular redox state. Similarly, HO-1 expression levels were increased in CYGB-depleted LY podocytes (Supplementary Fig. S2). To further confirm this observation, WT, shCTR and shCYGB AB8/13 cells were transiently transfected with the cytoplasmic oxidation-sensitive roGFP2-Orp1 probe. Compared to WT cells, shCYGB-1 and shCYGB-2 cells showed a significant increase in roGFP2-Orp1 oxidation under basal conditions (Fig. 4A), consistent with the gene expression data. Treatment with antimycin A (AMA), a mitochondrial complex III inhibitor, further increased roGFP2-Orp1 oxidation, particularly in the two shCYGB cell models (Fig 4A). As an independent approach to measure ROS generation in podocytes we employed H₂DCFDA, a fluorescent cell-permeable indicator of ROS. Immediately after AMA treatment, DCF fluorescence strongly increased in shCYGB-1 cells compared to WT and shCTR cells (Fig. 4B). To confirm the results with an independent ROS stimulus, cells were subjected to 250 μM H₂O₂ and DCF fluorescence was measured over a 4 h period. ROS accumulation rapidly increased in shCYGB-1 and shCYGB-2 cells, reaching the highest value after 4 h (Fig. 4C).

Since podocyte loss has been associated with hyperglycemia and subsequent increase in oxidative stress (63), cells were incubated with high glucose or mannitol (used as isotonic control) for 5 days. Treatment with high glucose (HG) significantly increased ROS accumulation (Fig. 4D) and cell death (Fig. 4E) in shCYGB-1 and shCYGB-2 cells compared to

WT cells, indicating a protective role of CYGB in oxidative stress-mediated cell death. On the other hand, overexpression of CYGB reduced ROS accumulation and oxidative stress as assessed by roGFP2-Orp1 oxidation and H₂DCFDA based assays upon different stimuli (Supplementary Fig. S4). Collectively, these data provide evidence for an anti-oxidative role of CYGB in podocytes.

CYGB deficiency alters expression of multiple genes involved in redox signaling and apoptosis.

The CYGB-dependent transcriptome was determined by RNA sequencing of shCTR and shCYGB-1 cells. Three independent samples for each condition were analyzed and the knockdown efficiency of shCYGB-1 was confirmed to be > 90% (Supplementary Fig. S5A). Most of the total reads mapped to exons (90%), whereas introns and intergenic regions accounted only for 9% and 1% of the total reads, respectively (Supplementary Fig. S5B), confirming the quality of the multiple mapping. Furthermore, sample-to-sample distance and principal component analysis of the RNA-seq datasets indicate clear separation among shCYGB and shCTR cells (Supplementary Fig. S5C-D).

To ascertain the reliability of the sequenced samples the transcriptomics data were compared with podocyte-specific marker genes based on literature search and single cell RNA sequencing (scRNA-seq) (39). Genes were considered to be expressed in the shCTR and shCYGB AB8/13 datasets if the mean RPKM value were ≥ 0.1 and ≥ 0.5 , respectively (39). In shCTR AB8/13 cells 83-95% of the literature-based (RPKM ≥ 0.5 = 68/82; RPKM ≥ 0.1 = 72/82) and 76-82% of the scRNA-seq-based (RPKM ≥ 0.5 = 58/76; RPKM ≥ 0.1 = 62/76) essential podocyte genes were expressed (Supplementary Tables 3 and 4) thereby validating that AB8/13 cells represent a genuine podocyte model.

More than 1500 genes were found differentially expressed in shCYGB compared to shCTR cells (Fig. 5A) and among these, the majority (1148) was downregulated. The most significantly upregulated genes included *UBD* (Ubiquitin D), *UGT1A6* (UDP Glucuronosyltransferase Family 1 Member A6) and *NPY4R* (Neuropeptide Y Receptor Y4) whereas the most significantly downregulated genes included *ARC* (Activity Regulated Cytoskeleton Associated Protein), *HS6ST2* (Heparan Sulfate 6-O-Sulfotransferase 2) and *MAFB* (MAF BZIP Transcription Factor B). To investigate if the observed differentially expressed genes are associated with common canonical pathways based on established

interactions among them, an Ingenuity Pathway Analysis (IPA) was carried out. Interestingly, differentially expressed genes could be attributed to multiple kidney failure associated pathways (Supplementary Table 5). Additionally, by using the CLC Genomics Workbench 8.5.1 RT² Profiler gene lists (Qiagen) we observed an association of the CYGB-dependent transcriptome with apoptosis and oxidative stress pathways (Supplementary Table 6). Using similar RT² Profiler gene lists as well as GO, KEGG and IPA tools we also specifically looked at metabolism associated genes but no clear enrichments could be observed (data not shown). Furthermore, analysis of expression levels of candidate metabolism associated genes in whole kidney extracts of *Cygb*^{+/+} and *Cygb*^{-/-} mice did not reveal any apparent differential regulation *in vivo* (Supplementary Fig. S1E).

In line with the increased oxidative stress and apoptosis of CYGB-depleted AB8/13 cells, several anti-oxidant genes such as *DUOX-1*, *DUOX-2*, and *GPX-3*, as well as some anti-apoptotic genes, like TP73, were found to be downregulated. Furthermore, multiple genes indicating podocyte injury, including *SERPINE1* and *CTGF*, were upregulated (Table 1). To validate the most relevant differentially expressed genes we performed RT-qPCR on independent RNA samples of shCYGB and shCTR AB8/13 cells (Fig. 5B). A similar CYGB-dependent regulation of *DUOX-1*, *GPX-3* and *SOD3* was found in LY cells, validating the results observed in AB8/31 (Fig. 5C). In contrast, a selection of redox-sensitive genes was not differentially regulated in whole kidney lysates of *Cygb*^{+/+} and *Cygb*^{-/-} mice (Supplementary Fig. S1F). Consistently, levels of protein carbonyls in whole kidney lysates from *Cygb*^{+/+} and *Cygb*^{-/-} mice were comparable, suggesting the absence of apparent differences in ROS levels *in vivo* (Supplementary Fig. S1G). Of particular interest is the downregulation of WT-1 and MAFB, both established regulators of podocyte development and viability in shCYGB AB8/13 cells versus shCTR cells. A similar, albeit less pronounced, downregulation of WT-1 and MAFB could be observed in stably CYGB-depleted LY cells (Fig. 5C). To confirm this CYGB-dependent regulation on protein level we carried out immunoblotting for both proteins. Immunoblotting experiments clearly recapitulated the obtained RNA results, illustrating reduced protein expression of WT-1 and MAFB in CYGB-deficient AB8/13 cells compared to shCTR cells (Fig. 5D). A comparable trend could be observed in CYGB-deficient LY cells (Fig. 5E). Finally, we also evaluated MafB expression levels in whole kidney lysates of *Cygb*^{+/+} and *Cygb*^{-/-} mice, demonstrating reduced renal

MafB mRNA and protein levels in *Cygb*-deficient mice (Supplementary Fig. S6B-C). Collectively, analysis of the *CYGB*-dependent transcriptome in AB8/13 cells revealed altered expression of multiple genes involved in redox signaling and apoptosis as well as essential factors of podocyte biology, consistent with the *CYGB*-dependent phenotype.

CYGB is associated with CKD

Genome-wide association studies (GWAS) have proven to be a powerful tool in identifying novel genetic markers involved in CKD (50). By using GWAS databases (3) we identified a single-nucleotide polymorphism (SNP), located in an intergenic region 3' of the *CYGB* gene associated with albuminuria (Fig. 6A). UCSC-integrated ENCODE data (10) illustrate that the SNP (rs8082416) is localized in a DNaseI hypersensitivity cluster observed in 115 cell types that reflects open chromatin, and overlaps with strong transcription factor occupancy (Supplementary Fig. S7A). ChIP-sequencing datasets further revealed histone marks for an active enhancer (H3K4Me1) and basal components of the transcriptional machinery (RNA pol2 in cell lines SK-N-MC, IMR90 and HCT-116; as well as p300 in H1-hESC cells) in this region. Additionally, RNA polymerase II-associated ChIA-PET (chromatin interaction analysis by paired-end tag sequencing) data in MCF-7 cells from ENCODE suggested DNA looping of this potential enhancer region to the first intron of the *CYGB* gene, close to its transcription initiation site. To experimentally validate a potential synergistic action between this potential 3'-enhancer and the *CYGB* promoter we performed luciferase reporter gene assays. Whereas a 90 bp fragment of the 3'-enhancer spanning the SNP did not regulate heterologous SV40 promoter-driven luciferase activity, the 3'-enhancer substantially increased endogenous *CYGB* promoter-driven luciferase activity (Supplementary Fig. S7B), confirming a cooperation between the downstream enhancer and the *CYGB* promoter. However, the SNP site did not directly alter transcriptional activity of the *CYGB* gene under basal conditions as no change in luciferase activity could be observed between WT and mutated 3'-enhancer driven construct (Supplementary Fig. S7B).

As an independent approach, existing gene array data from human renal biopsy specimens collected from the European Renal cDNA Bank (8) were analyzed. Data were obtained from Affymetrix HG-U133 Plus 2.0 microarrays, hybridized with glomerular and

tubulointerstitial cDNA procured from different nephropathies as well as pre-transplant biopsies from living renal allograft donors as controls. These biopsy expression studies from CKD patients revealed a consistent association of CYGB expression levels with advanced end-stage CKD, including diabetic nephropathy (Fig. 6B). CYGB mRNA levels in different kidney diseases were validated by RT-qPCR in an independent patient cohort, supporting the association of increased CYGB mRNA levels with diabetic nephropathy (Fig. 6C). In summary, these data suggest an association of CYGB with CKD.

DISCUSSION

Based on *in vivo* and *in vitro* data we propose that *Cygb* has a previously underappreciated role in podocyte function. Our study demonstrates that *Cygb* is expressed in mouse glomeruli, is important to preserve basal renal function possibly via a podocyte-related role and can protect podocytes from oxidative stress and cell death under various experimental conditions *in vitro*. Specifically, CYGB-deficient podocytes display increased ROS accumulation and apoptosis, as well as dysregulation of multiple genes involved in cellular redox balance, apoptosis and podocyte integrity. Additionally, we provide evidence for an association of CYGB with CKD using patient biopsies.

Whereas the anti-oxidative function of CYGB has reached a consensus in the globin field, the precise molecular mechanism underlying this function is still poorly understood. Most likely CYGB may scavenge ROS using heme and thiol residues (13,51), while peroxidase and superoxide dismutase activity have been excluded by the investigations of Trandafir and co-workers (68). In an attempt to investigate the molecular mechanism in more depth, we explored the function of CYGB in various renal cell models. To the best of our knowledge a role of CYGB in podocytes has not been investigated, so far. Consistent with the RNA-sequencing based results of micro-dissected renal tubules from Lee et al. (32), the studies by Geuens and colleagues (18) and the recent results of Balkawade and coworkers (1) we detected high levels of *Cygb* protein in mouse glomeruli (Fig. 1A). *Cygb*-deficient mice displayed a reduced number of podocytes (Fig. 1E). Consistently, renal function, as measured by FITC-sinistrin clearance, was reduced in *Cygb*-deficient mice (Fig. 1D). Mechanistic studies in two cellular models of podocytes, which express more abundant endogenous CYGB levels compared to any other kidney-derived cell lines (Fig. 2A), validate

an anti-oxidative function of CYGB. CYGB depletion, employing independent shRNA targeting sequences (Fig. 2D-E), induced increased cell death as measured by trypan blue exclusion (Fig. 3A) and cleaved PARP (Fig. 3B), an established apoptosis marker as well as DNA damage (Fig. 3C), corroborating with the previously observed anti-apoptotic role of CYGB (14,31,60,61). Using complementary methods we show that podocytes with attenuated CYGB expression display increased oxidative stress (Fig. 4A-E). In line with this observation, Seahorse-based analysis suggest impaired mitochondrial function in CYGB depleted cells as evidenced by reduced mitochondrial respiratory capacity (Fig. 3D-E). An NO dioxygenase function has been suggested for CYGB (17,24). As AB8/13 cells only express very low levels of NO synthases, an NO-mediated inhibiting effect of basal oxygen consumption rate following knockdown of CYGB, is very unlikely and rather argues for a ROS-dependent effect of altered mitochondrial respiratory capacity. CYGB overexpression on the other hand reduced oxidative stress, prevented ROS accumulation in AMA-treated podocytes and promoted cell viability, in line with previous findings (14,26,74). Podocyte apoptosis has been demonstrated as a cause of podocyte depletion (30). Similar to the phenotype of reduced number of podocytes observed in our *Cygb*^{-/-} mice, multiple pathologies such as diabetic nephropathy have been associated with loss of podocytes. Specifically, in diabetic nephropathy hyperglycemia-induced ROS accumulation was shown to contribute to podocyte apoptosis and depletion (35,63). Upon treatment with high glucose CYGB-deficient podocyte cells displayed increased ROS production and more pronounced cell death, compared to controls, strongly suggesting a protective role of CYGB. In contrast to our expectations we did not observe albuminuria or proteinuria in *Cygb*^{-/-} mice. Accordingly, Maclsaac and colleagues reported that absence of proteinuria not precludes loss of renal function (41). Alternatively, this lack might be due to the mild nature of the *Cygb* phenotype that, despite decreased podocyte number, is able to maintain filter barrier integrity or, in case it is not, may rely on enhanced proximal tubule endocytic activity resulting in compensating proximal tubular protein reabsorption. In support of the latter hypothesis increased megalin expression has recently been described in type 2 diabetes (4). Future studies are required to study if challenging conditions such as e.g. induction of diabetic nephropathy would lead to proteinuria in *Cygb*^{-/-} mice. According to the study of Susztak et al. (63) hyperglycemia-induced overproduction of ROS could

cause a diminution of the number of podocytes which could contribute to the development of diabetic nephropathy. Although CYGB knockout was sufficient to induce some histological changes such as podocyte loss, it was not sufficient to induce other histological changes as well as functional changes in the glomerulus (albuminuria). These changes may become apparent upon exposure to diabetic conditions and suggest a certain threshold of podocyte injury which is exacerbated under diabetic conditions. On the other hand, we cannot exclude a developmental defect in the *Cygb*^{-/-} mice.

Transcriptome analysis of CYGB-deficient podocytes and control cells revealed dysregulation of multiple genes involved in redox balance, apoptosis, podocyte function and podocyte injury (Fig 5A-B). Most of the genes were downregulated, indicating a general transcriptional repression in the absence of CYGB. As this could potentially hint to a decreased metabolic function we performed a close inspection of metabolism associated genes, but only could observe few moderate changes in gene expression, insufficient for explaining a decreased metabolic function. Similarly, a decrease in general mRNA stability upon lowered CYGB expression cannot be ruled out.

Due to its homology to Mb and their comparable O₂-binding affinity, CYGB was originally thought to contribute to the intracellular O₂ supply (69), acting as an O₂ reservoir or as signal transducer in O₂ sensing pathways (18,25). Therefore, CYGB deficiency would decrease oxygen availability and ROS signaling. DUOX-1 and DUOX-2 belong to the NADPH oxidases (NOX) family and need oxygen as co-substrate to produce ROS (i.e. H₂O₂ or O₂⁻). Both DUOX-1 and DUOX-2 are downregulated in lung cancer (40) and in hepatocellular carcinoma (DUOX-1) (34), in conditions where increased ROS levels were observed. However, their role in podocytes is still unknown. Downregulation of anti-oxidative genes, including CYGB, SOD3, GPX3 and GPX7 could explain the accumulation of ROS, as previously reported (60). The absence of differential expression of these anti-oxidative genes in whole kidney lysates of *Cygb*^{+/+} and *Cygb*^{-/-} mice might be explained by compensation of multiple other surrounding cell types.

Intriguingly, attenuated CYGB expression leads to downregulation of WT-1 and MAFB, essential podocyte transcription factors involved in maintaining cell differentiation (Fig. 5C-E). In line with these *in vitro* data both Wt-1 and MafB were downregulated in *Cygb*^{-/-} mice. WT-1 represents a key regulator of podocyte function and its downregulation leads

to glomerulonephritis and mesangial sclerosis (20). Various mutations in WT-1 cause podocytopathies, including Denys–Drash syndrome, Frasier syndrome, and non-syndromic focal segmental glomerulosclerosis (43). Whereas major efforts have focussed on the identification of transcriptional targets of WT-1 in podocytes, the finding of an upstream regulator is of substantial interest, as well. Moreover, WT-1 promotes expression of a large subset of the podocyte proteome, probably by activating the transcription of other transcriptional regulators that act either cooperatively with or independently of WT-1 (43). Studies by Dong et al. (11) provided evidence that WT-1 represents a crucial transcription factor for podocyte maturation and maintenance and fulfills its function by regulation of various target genes, including *Nphs2*, *Mafb* and *Magi2*. In line with the differential regulation of WT-1 in CYGB-depleted podocytes as well as in *Cygb*^{-/-} mice, we found that these target genes are CYGB-dependently regulated in podocytes. Particularly, MAFB, a WT-1 key target gene has been shown as well to be essential for kidney development (45). Furthermore, its overexpression in podocytes protects against diabetic nephropathy, through the regulation of slit diaphragm proteins, anti-oxidative enzymes, and the Notch pathway (46). Additionally, LMX1B a transcription factor crucial for proper differentiation of podocyte precursors, was shown to be downregulated in CYGB-deficient podocytes. Overall, our RNA-seq-based transcriptome data in a AB8/13 cell model illustrate that CYGB influences multiple crucial transcription factors in podocyte biology, indicate its potential relevance to podocytopathies and suggest that CYGB might therefore represent a potential therapeutic target.

Using GWAS we discovered a SNP in the 3' intergenic region of the *CYGB* gene, potentially associated with increased albuminuria (Fig. 6A). The SNP coincides with a region displaying several hallmarks of an enhancer and loops back to the first intron of *CYGB* gene close to the transcription initiation site as indicated by ChIA-PET data. Consistent with the chromatin looping data, reporter gene assays provide evidence for a cooperation between the distal downstream 3'-enhancer and the proximal *CYGB* promoter in regulating *CYGB* expression. Although additional studies under experimental conditions would be required to validate a potential direct effect of the SNP on *CYGB* gene regulation, these experiments indicate a further correlation of the SNP and the *CYGB* gene locus. Intriguingly, this is the first time that a globin gene was associated with CKD. Simultaneously, the potential role of

CYGB in acquired human renal disease was found in an unbiased way by analyzing transcriptomic data of patients with different stages of renal failure (Fig. 6B-C).

In conclusion, our study demonstrates that CYGB (i) is abundantly expressed in human podocyte cell lines, (ii) protects podocytes from oxidative stress and apoptosis, (iii) is required to preserve renal function possibly via a podocyte-associated protective role and (iv) is implicated in CKD.

INNOVATION

CYGB represents the fourth recently identified globin in humans. The renal role of CYGB has not been extensively explored. Our findings indicate a previously undiscovered podocyte-related renal role of *Cygb*, confirm abundant CYGB expression in human podocyte cell lines, provide evidence for an anti-oxidative role of CYGB in podocytes and describe for the first time an association between CYGB and chronic kidney disease.

MATERIALS AND METHODS

Reagents

Antimycin A (AMA; Sigma-Aldrich, St Louis, MO, USA) was dissolved in 95% ethanol. H₂O₂ was purchased from Sigma-Aldrich. 2'7'-Dichlorodihydrofluorescein diacetate (H₂DCFDA) (10 μM; Invitrogen, Thermo Fischer Scientific, Waltham, MA, USA) was dissolved in DMSO. 3-(4,5-dimethylthiazol-2-yl)-2,5-diphenyltetrazoliumbromide (Sigma-Aldrich) for MTT assays was dissolved in PBS. For the analysis of human renal biopsies, TaqMan reagents for human *CYGB* (NM_134268) were purchased from Applied Biosystems (Waltham, MA, USA). D-glucose solution and D-mannitol were purchased from Sigma-Aldrich. OxyBlot protein oxidation kit (S7150) was purchased from Sigma-Aldrich. Hematoxylin and eosin solutions were purchased from Sigma-Aldrich.

Renal function analysis and tissue sampling of *Cygb*-deficient mice

C57BL/6 *Cygb* global knockout mice were generated as described previously (64). To evaluate whether there was a difference in baseline renal function as compared to wild type C57BL/6, glomerular filtration rate (GFR) was determined by measuring FITC-sinistrin clearance. FITC-sinistrin is a fluorescent inulin analogue, which is only excreted via glomerular filtration (52). For these experiments, 9 male *Cygb*^{+/+} and 9 male *Cygb*^{-/-} mice

16

(age 18 weeks) were implanted with 2 osmotic minipumps (model 1002, release rate of 0.25 $\mu\text{l/h}$ for 14 days; Alzet, Charles River, Beerse, Belgium) filled with 100 mg/ml FITC-sinistrin (Fresenius Kabi Austria GmbH, Linz, Austria), two weeks before sacrifice. Mice were anesthetized via intraperitoneal injection with a mixture of ketamine (80 mg/kg) and xylazine (16 mg/kg) in 0.9% NaCl and kept on a heating pad (37°C) during surgery. After midline depilation with Veet creme and skin sterilization with ethanol, a ventrolateral incision (0.5 cm) was made and pumps were placed into the peritoneal cavity. The incision was closed with sterile suture, muscle and skin separately. Mice regained consciousness and mobility under partial exposure to a heating lamp, after which they were put into their housing cages. The two pump strategy was based on the report of Qi et al. assuring sufficient serum FITC-sinistrin levels for renal function assessment (54). For final GFR calculation, we applied the equation "FITC-sinistrin clearance = FITC-sinistrin pump infusion rate/steady-state blood FITC-sinistrin concentration" (54).

Twenty-four hours before sacrifice, mice were put in metabolic cages with free access to water and food for 24 h urine collection. Urine was stored at -20°C until further analyses. At sacrifice, mice were deeply anesthetized and exsanguinated via the vena cava inferior for blood collection. Serum was extracted and kept at -20°C for further analyses. Kidneys were isolated, decapsulated, weighed, sliced in 1mm transverse sections and snap frozen in liquid nitrogen or fixed in Neutral Buffered Formalin (NBF). Urine and serum parameters Na^+ - and K^+ - concentrations were determined using an electrolyte analyzer (IL-943, Instrumentation Laboratories, Bedford, MA, USA). Osmolality was measured using the Fiske One-Ten osmometer (Fiske, Norwood, MA, USA). Albuminuria was assessed by loading 5 μl of urine sample on a polyacrylamide gel and bovine serum albumin (BSA) was used as positive control.

All experimental procedures were performed in accordance with the National Institutes of Health Guide for the Care and Use of Laboratory Animals and approved by the University of Antwerp Ethical Committee (permit 2016-47).

Immunohistochemistry

Paraffin-embedded kidney sections were deparaffinized, hydrated, blocked, and incubated overnight with anti-Wt-1 (ab89901, Abcam, Cambridge, UK). After washing, sections were incubated with a biotinylated goat anti-rabbit IgG antibody (Vector Laboratories, Burlingame, California) and subsequently incubated with avidin and biotinylated horseradish peroxidase (Vector Laboratories). A dark brown color was developed with diaminobenzidine in the presence of 3% H₂O₂. Sections were counterstained with hematoxylin and eosin and mounted in Eukitt (Sigma-Aldrich). Podocyte counts were assessed by staining kidney sections for Wt-1 and quantification was performed in a blinded manner. Glomerular diameters of 30 glomeruli/section were measured from five mice per experimental group using ImageJ. Glomerular volume was determined as $Gv = \beta / k \cdot (\pi \cdot r^2)^{3/2}$, where $\beta = 1.38$ is the shape coefficient for spheres, $k = 1.1$ is the size distribution coefficient, and $(\pi \cdot r^2)$ is the glomerular area (58). For immunofluorescence experiments Cygb staining on Cygb^{+/+} and Cygb^{-/-} kidneys was performed using anti-Cygb (D-7, sc365246, Santa Cruz Biotechnology, Dallas, TX, USA) and the Vector mouse on mouse (M.O.M.) Immunodetection kit, fluorescein (FMK-2201, Vector Laboratories) according to the manufacturer's instructions. Subsequently, sections were mounted with DAPI Fluoromount-G (SouthernBiotech, Birmingham, AL, USA) and visualized using fluorescence microscopy.

Cell culture and treatments

Conditionally immortalized human podocyte cell lines AB8/13 and LY were a kind gift from A. Kistler (57). Cells were cultured in RPMI (Sigma-Aldrich) supplemented with 10% heat-inactivated fetal calf serum (FCS; Gibco, Thermo Fischer Scientific), 50 IU/ml penicillin, 50 µg/ml streptomycin (Invitrogen), 5 µg/ml insulin, 5 µg/ml transferrin, and 5 ng/ml sodium selenite (ITS; Roche, Mannheim, Germany). AB8/13 cells were propagated at 33°C and differentiated for 10-14 days at 37°C in a humidified incubator containing 5% CO₂ (Binder, Tuttlingen, Germany). Cell death was measured by the Vi-Cell XR 2.03 Cell Viability Analyzer (Beckman Coulter, Krefeld, Germany) and TC20 automated cell counter (BioRad) using the trypan blue dye exclusion method. HPRT, HEK293T, TK-173, TK-188 and TZ-1 cells were cultured in high glucose DMEM (Sigma-Aldrich) supplemented with 10% heat-

inactivated FCS, 50 IU/ml penicillin and 50 µg/ml streptomycin (Invitrogen). HK-2 were cultured in DMEM/F12 (Sigma-Aldrich) supplemented with 10% heat-inactivated FCS, 100 U/ml penicillin, 100 µg/ml streptomycin, 36 ng/ml hydrocortisone, 5 µg/ml insulin, 5 µg/ml transferrin and 5 ng/ml selenium (ITS) solution (Roche).

mRNA and protein detection and quantification

Total cellular RNA was extracted as previously described (29). Total RNA (2 µg) was reverse transcribed (RT) using the Prime Script RT reagent kit (Takara Bio USA) and complementary DNA (cDNA) levels were estimated by quantitative polymerase chain reaction (qPCR) using the primers listed in Supplementary Table 1 and a SYBRGreen qPCR reagent kit (Sigma-Aldrich) in a CFX96 C1000 Thermal Cycler (BioRad). Transcript levels were calculated as described before (28) and displayed as fold change, if not otherwise indicated.

Immunoblotting, signal imaging and quantification were performed as previously reported (47). Membranes were probed with antibodies against CYGB (13317-AP Proteintech, Rosemont, IL, USA; or EPR13198, Abcam, Cambridge, UK), Synaptopodin (SYNPO) (P-19, sc-21537, Santa Cruz Biotechnology), PARP1 ([E102], ab32138, Abcam), cleaved PARP1 ([E51], ab32064, Abcam), TATA-box binding protein (TBP) (8515, Cell Signaling Technology, Leiden, The Netherlands), β-Actin (A5441, Sigma-Aldrich) and α-Tubulin (TU-02, sc-8035, Santa Cruz Biotechnology). Signals from HRP-coupled secondary antibodies were detected with ECL substrate (Pierce, Thermo Fisher Scientific) using a luminescent image analyzer (Fusion FX6, Vilber Lourmat, Marne la Vallée, France). Uncropped immunoblots are provided in Supplementary Figure S8. Protein oxidation was detected by the OxyBlot method following the manufacturer's instructions. Briefly, each specimen was divided in two aliquots: one aliquot was subjected to derivatization reaction (2,4-Dinitrophenylhydrazine DNPH Solution), while the other one served as a negative control (Derivatization-Control Solution). The treated samples and the corresponding negative control were loaded into a polyacrylamide gel. After gel electrophoresis, transfer and blocking, the membrane was incubated with primary antibody specific to the dinitrophenyl (DNP) moiety of the proteins, HRP-coupled secondary antibody and finally exposed on autoradiography film.

Generation of stable knock-down and overexpression cell lines

Expression vectors encoding short hairpin RNA (shRNA) sequences targeting human CYGB in a pLKO.1-puro plasmid were purchased from Sigma-Aldrich (shCYGB-1: order number TRCN0000059378; shCYGB-2: order number TRCN0000059381). Control cells (shCTR) were transfected with a non-targeting control shRNA under the control of a U6 promoter in a pLKO.1 puromycin resistance vector (Sigma-Aldrich) as described previously (16). Viral particles were produced in HEK293T cells by co-transfection of the respective transfer vector (3 µg) with the packaging plasmids pLP1 (4.2 µg), pLP2 (2 µg) and pVSV-G (2.8 µg, all from Invitrogen) using polyethylenimine (PEI) transfection as described before (15). Cells were transduced with lentiviral-pseudotyped particles and cell pools were cultured with the appropriate antibiotic for selection. For stable overexpression full-length human *CYGB* gene and control gene β -glucuronidase (*GUS*) were cloned into a pLENTI6 plasmid. Viral particles were produced as described above.

H₂DCFDA assay

AB8/13 cells were seeded in 96-well plates at 80% confluency and incubated with 10 µM H₂DCFDA for 30 min in the dark. Fluorescence was measured using a 96-well fluorometer (Infinite 200Pro, Tecan, Männedorf, Switzerland). Results from kinetics measurements were calculated as described previously (21). Analysis was performed using the internal software i9 control.

roGFP2-Orp1 measurements

AB8/13 cells were grown on glass bottom dishes (Ibidi GmbH, Martinsried, Germany) and transduced with the H₂O₂-sensitive probe roGFP2-Orp1 (22,44), which was subcloned into the pAd/CMV/V5-DEST adenoviral vector (Invitrogen) using the Gateway technology. After 48 h, the oxidation of the sensor was measured at basal level or upon AMA treatment (50 µg/ml, 30 min). The live measurements of roGFP2 oxidation and calculations of the degree of oxidation were performed as previously described (70).

Cell viability assay

For the MTT assay, AB8/13 cells were seeded in 96-well flat bottom plates and then exposed to AMA or H₂O₂ at the indicated concentrations (final volume 0.1 ml per well).

20

After 6 h, 10 μ l of 5 mg/ml MTT solution in PBS were added for 2 h. Following removal of the medium, 100 μ l of DMSO were added to dissolve the formazan crystals. The absorbance at 540 nm was determined in triplicates using a plate reader (Infinite 200Pro, Tecan) and normalized by non-treated cells.

TUNEL assay

Cells were seeded on coverslips and treated with 250 μ M H₂O₂ for 3 h. Terminal deoxynucleotidyl transferase dUTP nick end labeling (TUNEL) of nuclei was performed by using the APO-BrdU *in situ* DNA fragmentation assay kit (K401-60; Biovision, Milpitas, CA, USA) following the manufacturer's protocol.

Determination of Cellular Bioenergetics

Differentiated human podocytes were seeded on XF^e24-well microplates (Agilent technologies, Santa Clara, CA, USA) at 1.5×10^4 cells per well and incubated at 37 °C and 5% CO₂ the day before the experiment. The medium was then replaced by RPMI 1640 without bicarbonate, and cells were kept in an incubator without CO₂ before transfer to a Seahorse analyzer XF^e24 (Agilent Technologies), to measure the O₂ consumption rate (OCR). Three measurements of OCR were performed at steady state and after sequential injection of 1 μ M oligomycin, 2 μ M FCCP and a mix of 0.5 μ M rotenone and 0.5 μ M AMA. During the experiment, the cells were kept in a humidified chamber at 37°C, under normal oxygen conditions. At the end of the assay, total protein per well was measured using Bradford reagent (BioRad, Hercules, CA, USA) and OCR values were normalized to the protein amount.

Analysis of human renal biopsies

Human renal biopsy specimens and Affymetrix microarray expression data (HG-U133 Plus2.0 Array; Affymetrix, Santa Clara, CA, USA) were obtained within the framework of the European Renal cDNA Bank–Kröner-Fresenius Biopsy Bank (8). Diagnostic renal biopsies were obtained from patients after informed consent and with approval of the local ethics committees. Following renal biopsy, the tissue was transferred to RNase inhibitor and microdissected into glomerular (Glom) and tubulointerstitial (Tub) compartments. The microarray expression data used in this study came from individual

patients with diabetic nephropathy (DN, Glom ($n = 7$), Tub ($n = 7$), focal segmental glomerulosclerosis (FSGS, Glom ($n = 16$), Tub ($n = 7$)), rapidly progressive glomerulonephritis (RPGN, Glom ($n = 23$), Tub ($n = 21$)), minimal change disease (MCD, Glom ($n = 5$), Tub ($n = 5$)) as well as pre-transplant biopsies from living renal allograft donors as controls (LD, Glom ($n = 18$), Tub ($n = 18$)). Total RNA was isolated from microdissected glomeruli and tubulointerstitium, reverse transcribed, and linearly amplified according to a protocol previously reported (9). Fragmentation, hybridization, staining and imaging were performed following the Affymetrix expression analysis technical manual (Affymetrix). The raw data was normalized using Robust Multichip Algorithm (RMA) and annotated by Human Entrez Gene custom CDF annotation version 18 (<http://brainarray.mbni.med.umich.edu/Brainarray/default.asp>). To identify differentially expressed genes the SAM (Significance analysis of Microarrays) method was applied using TiGR (MeV, Version 4.8.1) (71). A q -value below 5% was considered to be statistically significant. RT-qPCR validation of renal biopsies was performed as reported earlier (8,59). Pre-developed TaqMan reagents were used for human *CYGB* (NM_134268) and transcript levels were normalized to β -Actin levels ((LD, Glom ($n = 9$), Tub ($n = 5$), (DN, Glom ($n = 12$), Tub ($n = 15$), focal segmental glomerulosclerosis (FSGS, Glom ($n = 16$), Tub ($n = 17$)), rapidly progressive glomerulonephritis (RPGN, Glom ($n = 9$), Tub ($n = 9$)).

Genome-wide association study

Genetic association testing for urinary albumin-to-creatinine ratio (UACR) and meta-analysis was performed in the CKDGen and CARE cohorts of European ancestry, with further follow-up genetic analysis of significant SNPs in CARE cohorts of African-American ancestry and in the Diabetes Control and Complications Trial/Epidemiology of Diabetes Interventions and Complications (DCCT/EDIC) Study, as previously described (3).

RNA-seq library preparation and transcriptome sequencing

Total RNA from three independent samples of shCTR and shCYGB-1 AB8/13 cells was extracted using the RNeasy mini kit according to manufacturer's instructions (Qiagen, Hilden, Germany). Prior to library construction, RNA quality was assessed using an Agilent 2100 Bioanalyzer and the Agilent RNA 6000 Nano Kit (Agilent Technologies, Santa Clara,

CA, USA). RNA Integrity Number (RIN) values ranged from 8.5 to 9.7, indicating high quality RNA samples. RNA was quantified using Qubit RNA HS Assay Kit (Invitrogen). Libraries were prepared starting from 800 ng of total RNA using the TruSeq Stranded mRNA HT Sample Prep Kit (Illumina) including a poly-A selection step following the manufacturer's instructions and sequenced as 2 x 150 nt paired-end reads using an Illumina NextSeq 500™. Library preparation and sequencing were performed by StarSEQ® GmbH (Mainz, Germany). RNA-Seq data are available at the European Nucleotide Archive under accession number PRJEB30641.

Differential gene expression, GO term annotation and pathway enrichment analyses

Raw sequences were pre-processed to remove low quality reads and residual Illumina adapter sequences using FASTX-Toolkit 0.0.14 (http://hannonlab.cshl.edu/fastx_toolkit/). The overall sequencing quality and the absence of adapter contamination were evaluated with FastQC 0.11.2 (<http://www.bioinformatics.babraham.ac.uk/projects/fastqc/>). Pre-processed reads were mapped against the annotated human genome version *hg38* with the RNA-seq algorithm of CLC Genomics Workbench 8.5.1 using the following parameters: mismatch cost = 2, insertion cost = 3, deletion cost = 3, length fraction = 0.95, and similarity fraction = 0.95. The mapping step was performed allowing either one (single) or up to 10 (multiple) mappings for each read, and all the downstream statistical and bioinformatical analyses were computed for both mapping outputs. As the results of the downstream analyses for single or multiple mapping converged (data not shown), only the results obtained with multiple mapping (the library of 2 x 150 nt paired-end stranded reads minimizes the occurrence of unspecific read mappings) were included. A summary of the mapping statistics is shown in Supplementary Table 2. Principal Component Analysis (PCA) was performed and visualized using the plotPCA function of DESeq2 (38) (ntop=1000) and ggplot2 (73) R packages (Supplem. Fig. 5C-D). Sample-to-sample distance was calculated from the transformed count matrices and visualized as heatmap using the Pheatmap R package. Both approaches indicated a clear separation among the shCTR- and shCYGB-derived datasets. In particular, PC1 accounted for 87% of the variance.

Differentially expressed genes were determined using the EdgeR-based (Empirical analysis of DGE; (55,56) statistical tool of CLC Genomics Workbench using default parameters. Genes were considered differentially expressed when presenting $|\text{fold change}| > 2$ and false discovery rate (FDR)-corrected $p\text{-value} \leq 0.05$. GO term and KEGG pathway enrichment analyses were performed using WebGestalt (version 2017, <http://bioinfo.vanderbilt.edu/webgestalt/>) using the Overrepresentation Enrichment Analysis method, requiring a BH-corrected $p\text{-value} \leq 0.05$ and a minimum enrichment of 4 genes for term/pathway. Enrichment in Canonical Pathways and Tox Functions were performed with Qiagen's Ingenuity Pathway Analysis (IPA, Qiagen) Core analysis tool using bias-corrected z-score (when applicable) and BH-corrected $p\text{-values} \leq 0.05$.

Luciferase reporter gene assays

A 90 bp oligonucleotide encompassing the rs8082416 SNP was cloned into pGL3prom (Promega) between the MluI and XhoI restriction sites. The CYGB promoter was amplified by PCR from genomic DNA of HEK293T cells and cloned into pGL3basic (Promega). If not otherwise indicated, 3×10^5 HEK293T cells were transiently transfected with 500 ng reporter plasmid in a six-well format using Rotifect (Carl Roth, Karlsruhe, Germany). To control for differences in transfection efficiency and extract preparation, 5 ng pRL-SV40 *Renilla* luciferase reporter vector (Promega) was co-transfected. Cultures were evenly split onto 24-well plates 24 hours after transfection. Luciferase activities of triplicate wells were determined using the Dual Luciferase Reporter Assay System (Promega) as described before (62). Reporter activities were expressed as relative firefly/*Renilla* luciferase activities. All reporter gene assays were performed at least 3 times independently.

Statistical analyses

If not otherwise indicated, results are presented as mean values \pm standard error of the mean (SEM) of at least three independent experiments. Statistical analyses were performed using Student's t-test and one-way ANOVA or two-way ANOVA where appropriate. $p\text{-values} < 0.05$ were considered statistically significant. For the human biopsy data statistical analysis was performed using Kruskal-Wallis and Mann-Whitney (SPSS 24.0, SPSS Inc., Chicago, IL) Test.

ACKNOWLEDGEMENTS

We thank Gerhard Müller and Michael Zeisberg for providing TK173, TK188 and TZ-1 cells, Moin Saleem for providing two podocyte cell lines, Caroline Fox, Ming-Huei Chen and the CKDGen Consortium for interrogating UACR datasets, Patrick D’Haese and Jean-Pierre Montani for advice, Julia Birk and Marcel Saarbeck for cloning assistance, Joey De Backer as well as all Hoogewijs laboratory members for advice and technical support. We also thank the participating centers of the European Renal cDNA Bank-Kröner-Fresenius biopsy bank (ERCB-KFB) and their patients for their cooperation. This work was supported by the Swiss National Science Foundation (grant 173000) and the German Research Foundation (grant HO5837/1-1) to D.H., a University Research Priority Program “Integrative Human Physiology” grant to E.B.R., the Biobank ERCB-KFB (Else Kröner-Fresenius-Foundation) to C.D.C., an intramural grant (Center for Computer Sciences, JGU Mainz) to T.H., the International PhD Program (IMB Mainz) to E.P. and T.H., a Grant-in-Aid for Scientific Research from JSPS (No. 25293177 and No. 16H05290) and a Grant for Research Program on Hepatitis from the Japan Agency for Medical Research and Development (AMED – 18fk0210004h0003) to NK, and the NCCR Kidney.CH financed by the SNF to C.D.C., O.D., A.O., R.H.W and D.H.

Author Disclosure Statement

All the authors declared no competing interests.

LIST OF ABBREVIATIONS

AMA = antimycin A

BH = Benjamini–Hochberg

CKD = chronic kidney disease

ChIA-PET = chromatin interaction analysis by paired-end tag sequencing

CYGB/Cygb = human/mouse cytoglobin

DCF = 2',7'-dichlorofluorescein

DN = diabetic nephropathy

FCCP = carbonyl cyanide-4 trifluoromethoxy phenylhydrazone

FDR = false discovery rate

FSGS = focal segmental glomerulosclerosis

GFR = glomerular filtration rate

GUS = β -glucuronidase

GWAS = Genome-wide association studies

H₂DCFDA = 2',7'-dichlorodihydrofluorescein diacetate

HO-1 = heme oxygenase 1

IPA = Ingenuity pathway analysis

Mb = myoglobin

MCD = minimal change disease

MTT = *3-(4,5-dimethylthiazol-2-yl)-2,5-diphenyltetrazoliumbromide*OCR = O₂ consumption rate

ROS = reactive oxygen species

RPGN = rapidly progressive glomerulonephritis

RPKM = reads per kilobase per million mapped reads

scRNA-seq = single cell RNA-sequencing

SNP = single-nucleotide polymorphism

REFERENCES

1. Balkawade RS, Chen C, Crowley MR, Crossman DK, Clapp WL, Verlander JW, Marshall CB. Podocyte-specific expression of Cre recombinase promotes glomerular basement membrane thickening. *Am J Physiol Renal Physiol* 316: F1026-F1040, 2019.
2. Betz B, Conway BR. An Update on the Use of Animal Models in Diabetic Nephropathy Research. *Curr Diab Rep* 16: 18, 2016.
3. Böger CA, Chen MH, Tin A, Olden M, Kottgen A, de Boer IH, Fuchsberger C, O'Seaghda CM, Pattaro C, Teumer A, Liu CT, Glazer NL, Li M, O'Connell JR, Tanaka T, Peralta CA, Kutalik Z, Luan J, Zhao JH, Hwang SJ, Akyzbekova E, Kramer H, van der Harst P, Smith AV, Lohman K, de Andrade M, Hayward C, Kollerits B, Tonjes A, Aspelund T, Ingelsson E, Eiriksdottir G, Launer LJ, Harris TB, Shuldiner AR, Mitchell BD, Arking DE, Franceschini N, Boerwinkle E, Egan J, Hernandez D, Reilly M, Townsend RR, Lumley T, Siscovick DS, Psaty BM, Kestenbaum B, Haritunians T, Bergmann S, Vollenweider P, Waeber G, Mooser V, Waterworth D, Johnson AD, Florez JC, Meigs JB, Lu X, Turner ST, Atkinson EJ, Leak TS, Aasarod K, Skorpen F, Syvanen AC, Illig T, Baumert J, Koenig W, Kramer BK, Devuyst O, Mychaleckyj JC, Minelli C, Bakker SJ, Kedenko L, Paulweber B, Coassin S, Endlich K, Kroemer HK, Biffar R, Stracke S, Volzke H, Stumvoll M, Magi R, Campbell H, Vitart V, Hastie ND, Gudnason V, Kardina SL, Liu Y, Polasek O, Curhan G, Kronenberg F, Prokopenko I, Rudan I, Arnlov J, Hallan S, Navis G, Parsa A, Ferrucci L, Coresh J, Shlipak MG, Bull SB, Paterson NJ, Wichmann HE, Wareham NJ, Loos RJ, Rotter JI, Pramstaller PP, Cupples LA, Beckmann JS, Yang Q, Heid IM, Rettig R, Dreisbach AW, Bochud M, Fox CS, Kao WH. CUBN is a gene locus for albuminuria. *J Am Soc Nephrol* 22: 555-70, 2011.
4. Bryniarski MA, Yee BM, Jaffri I, Chaves LD, Yu JA, Guan X, Ghavam N, Yacoub R, Morris ME. Increased Megalin Expression in Early Type 2 Diabetes: Role of Insulin Signaling Pathways. *Am J Physiol Renal Physiol* 315: F1191–F1207, 2018.
5. Burmester T, Ebner B, Weich B, Hankeln T. Cytochrome: a novel globin type ubiquitously expressed in vertebrate tissues. *Mol Biol Evol* 19: 416-21, 2002.

6. Burmester T, Hankeln T. Function and evolution of vertebrate globins. *Acta Physiol (Oxf)* 211: 501-14, 2014.
7. Burmester T, Weich B, Reinhardt S, Hankeln T. A vertebrate globin expressed in the brain. *Nature* 407: 520-3, 2000.
8. Cohen CD, Frach K, Schlondorff D, Kretzler M. Quantitative gene expression analysis in renal biopsies: a novel protocol for a high-throughput multicenter application. *Kidney Int* 61: 133-40, 2002.
9. Cohen CD, Klingenhoff A, Boucherot A, Nitsche A, Henger A, Brunner B, Schmid H, Merkle M, Saleem MA, Koller KP, Werner T, Grone HJ, Nelson PJ, Kretzler M. Comparative promoter analysis allows de novo identification of specialized cell junction-associated proteins. *Proc Natl Acad Sci U S A* 103: 5682-7, 2006.
10. Davis CA, Hitz BC, Sloan CA, Chan ET, Davidson JM, Gabdank I, Hilton JA, Jain K, Baymuradov UK, Narayanan AK, Onate KC, Graham K, Miyasato SR, Dreszer TR, Strattan JS, Jolanki O, Tanaka FY, Cherry JM. The Encyclopedia of DNA elements (ENCODE): data portal update. *Nucleic Acids Res* 46: D794-D801, 2018.
11. Dong L, Pietsch S, Tan Z, Perner B, Sierig R, Kruspe D, Groth M, Witzgall R, Grone HJ, Platzer M, Englert C. Integration of Cistromic and Transcriptomic Analyses Identifies Nphs2, Mafk, and Magi2 as Wilms' Tumor 1 Target Genes in Podocyte Differentiation and Maintenance. *J Am Soc Nephrol* 26: 2118-28, 2015.
12. Fordel E, Thijs L, Martinet W, Lenjou M, Laufs T, Van Bockstaele D, Moens L, Dewilde S. Neuroglobin and cytoglobin overexpression protects human SH-SY5Y neuroblastoma cells against oxidative stress-induced cell death. *Neurosci Lett* 410: 146-51, 2006.
13. Fordel E, Thijs L, Martinet W, Schrijvers D, Moens L, Dewilde S. Anoxia or oxygen and glucose deprivation in SH-SY5Y cells: a step closer to the unraveling of neuroglobin and cytoglobin functions. *Gene* 398: 114-22, 2007.
14. Fordel E, Thijs L, Moens L, Dewilde S. Neuroglobin and cytoglobin expression in mice. Evidence for a correlation with reactive oxygen species scavenging. *FEBS J* 274: 1312-7, 2007.

15. Fuady JH, Bordoli MR, Abreu-Rodriguez I, Kristiansen G, Hoogewijs D, Stiehl DP, Wenger RH. Hypoxia-inducible factor-mediated induction of WISP-2 contributes to attenuated progression of breast cancer. *Hypoxia (Auckl)* 2: 23-33, 2014.
16. Fuady JH, Gutsche K, Santambrogio S, Varga Z, Hoogewijs D, Wenger RH. Estrogen-dependent downregulation of hypoxia-inducible factor (HIF)-2alpha in invasive breast cancer cells. *Oncotarget* 7: 31153-65, 2016.
17. Gardner AM, Cook MR, Gardner PR. Nitric-oxide dioxygenase function of human cytoglobin with cellular reductants and in rat hepatocytes. *J Biol Chem* 285: 23850-7, 2010.
18. Geuens E, Brouns I, Flamez D, Dewilde S, Timmermans JP, Moens L. A globin in the nucleus! *J Biol Chem* 278: 30417-20, 2003.
19. Gnudi L. Cellular and molecular mechanisms of diabetic glomerulopathy. *Nephrol Dial Transplant* 27: 2642-9, 2012.
20. Guo JK, Menke AL, Gubler MC, Clarke AR, Harrison D, Hammes A, Hastie ND, Schedl A. WT1 is a key regulator of podocyte function: reduced expression levels cause crescentic glomerulonephritis and mesangial sclerosis. *Human Molecular Genetics* 11: 651-659, 2002.
21. Gutsche K, Randi EB, Blank V, Fink D, Wenger RH, Leo C, Scholz CC. Intermittent hypoxia confers pro-metastatic gene expression selectively through NF-kappaB in inflammatory breast cancer cells. *Free Radic Biol Med* 101: 129-142, 2016.
22. Gutscher M, Sobotta MC, Wabnitz GH, Ballikaya S, Meyer AJ, Samstag Y, Dick TP. Proximity-based protein thiol oxidation by H₂O₂-scavenging peroxidases. *J Biol Chem* 284: 31532-40, 2009.
23. Ha H, Hwang IA, Park JH, Lee HB. Role of reactive oxygen species in the pathogenesis of diabetic nephropathy. *Diabetes Res Clin Pract* 82 Suppl 1: S42-5, 2008.
24. Halligan KE, Jourdeuil FL, Jourdeuil D. Cytoglobin is expressed in the vasculature and regulates cell respiration and proliferation via nitric oxide dioxygenation. *J Biol Chem* 284: 8539-47, 2009.

25. Hankeln T, Ebner B, Fuchs C, Gerlach F, Haberkamp M, Laufs TL, Roesner A, Schmidt M, Weich B, Wystub S, Saaler-Reinhardt S, Reuss S, Bolognesi M, De Sanctis D, Marden MC, Kiger L, Moens L, Dewilde S, Nevo E, Avivi A, Weber RE, Fago A, Burmester T. Neuroglobin and cytoglobin in search of their role in the vertebrate globin family. *J Inorg Biochem* 99: 110-9, 2005.
26. Hodges NJ, Innocent N, Dhanda S, Graham M. Cellular protection from oxidative DNA damage by over-expression of the novel globin cytoglobin in vitro. *Mutagenesis* 23: 293-8, 2008.
27. Hoogewijs D, Ebner B, Germani F, Hoffmann FG, Fabrizius A, Moens L, Burmester T, Dewilde S, Storz JF, Vinogradov SN, Hankeln T. Androglobin: a chimeric globin in metazoans that is preferentially expressed in Mammalian testes. *Mol Biol Evol* 29: 1105-14, 2012.
28. Hoogewijs D, Houthoofd K, Matthijssens F, Vandesompele J, Vanfleteren JR. Selection and validation of a set of reliable reference genes for quantitative sod gene expression analysis in *C. elegans*. *BMC Mol Biol* 9: 9, 2008.
29. Hoogewijs D, Vogler M, Zwenger E, Krull S, Zieseniss A. Oxygen-dependent regulation of aquaporin-3 expression. *Hypoxia (Auckl)* 4: 91-97, 2016.
30. Jefferson JA, Shankland SJ, Pichler RH. Proteinuria in diabetic kidney disease: a mechanistic viewpoint. *Kidney Int* 74: 22-36, 2008.
31. Latina A, Viticchiè G, Lena AM, Piro MC, Annicchiarico-Petruzzelli M, Melino G, Candi E. Δ Np63 targets cytoglobin to inhibit oxidative stress-induced apoptosis in keratinocytes and lung cancer. *Oncogene* 35: 1493–1503, 2015.
32. Lee JW, Chou CL, Knepper MA. Deep Sequencing in Microdissected Renal Tubules Identifies Nephron Segment-Specific Transcriptomes. *J Am Soc Nephrol* 26: 2669-77, 2015.
33. Li D, Chen XQ, Li WJ, Yang YH, Wang JZ, Yu AC. Cytoglobin up-regulated by hydrogen peroxide plays a protective role in oxidative stress. *Neurochem Res* 32: 1375-80, 2007.
34. Ling Q, Shi W, Huang C, Zheng J, Cheng Q, Yu K, Chen S, Zhang H, Li N, Chen M. Epigenetic silencing of dual oxidase 1 by promoter hypermethylation in human hepatocellular carcinoma. *Am J Cancer Res* 4: 508-17, 2014.

35. Liu BC, Song X, Lu XY, Li DT, Eaton DC, Shen BZ, Li XQ, Ma HP. High glucose induces podocyte apoptosis by stimulating TRPC6 via elevation of reactive oxygen species. *Biochim Biophys Acta* 1833: 1434-42, 2013.
36. Liu X, El-Mahdy MA, Boslett J, Varadharaj S, Hemann C, Abdelghany TM, Ismail RS, Little SC, Zhou D, Thuy LT, Kawada N, Zweier JL. Cytoglobin regulates blood pressure and vascular tone through nitric oxide metabolism in the vascular wall. *Nat Commun* 8: 14807, 2017.
37. Liu X, Follmer D, Zweier JR, Huang X, Hemann C, Liu K, Druhan LJ, Zweier JL. Characterization of the function of cytoglobin as an oxygen-dependent regulator of nitric oxide concentration. *Biochemistry* 51: 5072-82, 2012.
38. Love MI, Huber W, Anders S. Moderated estimation of fold change and dispersion for RNA-seq data with DESeq2. *Genome Biol* 15: 550, 2014.
39. Lu Y, Ye Y, Bao W, Yang Q, Wang J, Liu Z, Shi S. Genome-wide identification of genes essential for podocyte cytoskeletons based on single-cell RNA sequencing. *Kidney Int* 92: 1119-1129, 2017.
40. Luxen S, Belinsky SA, Knaus UG. Silencing of DUOX NADPH oxidases by promoter hypermethylation in lung cancer. *Cancer Res* 68: 1037-45, 2008.
41. MacIsaac RJ, Tsalamandris C, Panagiotopoulos S, Smith TJ, McNeil KJ, Jerums G. Nonalbuminuric renal insufficiency in type 2 diabetes. *Diabetes Care* 27: 195-200, 2004.
42. Mimura I, Nangaku M, Nishi H, Inagi R, Tanaka T, Fujita T. Cytoglobin, a novel globin, plays an antifibrotic role in the kidney. *Am J Physiol Renal Physiol* 299: F1120-33, 2010.
43. Miner JH. Podocyte biology in 2015: New insights into the mechanisms of podocyte health. *Nat Rev Nephrol* 12: 63-4, 2016.
44. Morgan B, Sobotta MC, Dick TP. Measuring E(GSH) and H₂O₂ with roGFP2-based redox probes. *Free Radic Biol Med* 51: 1943-51, 2011.
45. Moriguchi T, Hamada M, Morito N, Terunuma T, Hasegawa K, Zhang C, Yokomizo T, Esaki R, Kuroda E, Yoh K, Kudo T, Nagata M, Greaves DR, Engel JD, Yamamoto M, Takahashi S. MafB is essential for renal development and F4/80 expression in macrophages. *Mol Cell Biol* 26: 5715-27, 2006.

46. Morito N, Yoh K, Ojima M, Okamura M, Nakamura M, Hamada M, Shimohata H, Moriguchi T, Yamagata K, Takahashi S. Overexpression of Mafb in podocytes protects against diabetic nephropathy. *J Am Soc Nephrol* 25: 2546-57, 2014.
47. Müller-Edenborn K, Leger K, Glaus Garzon JF, Oertli C, Mirsaidi A, Richards PJ, Rehrauer H, Spielmann P, Hoogewijs D, Borsig L, Hottiger MO, Wenger RH. Hypoxia attenuates the proinflammatory response in colon cancer cells by regulating IkappaB. *Oncotarget* 6: 20288-301, 2015.
48. Nakatani K, Okuyama H, Shimahara Y, Saeki S, Kim DH, Nakajima Y, Seki S, Kawada N, Yoshizato K. Cytoglobin/STAP, its unique localization in splanchnic fibroblast-like cells and function in organ fibrogenesis. *Lab Invest* 84: 91-101, 2004.
49. Nishi H, Inagi R, Kawada N, Yoshizato K, Mimura I, Fujita T, Nangaku M. Cytoglobin, a novel member of the globin family, protects kidney fibroblasts against oxidative stress under ischemic conditions. *Am J Pathol* 178: 128-39, 2011.
50. O'Seaghda CM, Fox CS. Genome-wide association studies of chronic kidney disease: what have we learned? *Nat Rev Nephrol* 8: 89-99, 2011.
51. Petersen MG, Dewilde S, Fago A. Reactions of ferrous neuroglobin and cytoglobin with nitrite under anaerobic conditions. *J Inorg Biochem* 102: 1777-82, 2008.
52. Pill J, Kraenzlin B, Jander J, Sattelkau T, Sadick M, Kloetzer HM, Deus C, Kraemer U, Gretz N. Fluorescein-labeled sinistrin as marker of glomerular filtration rate. *Eur J Med Chem* 40: 1056-61, 2005.
53. Qi Z, Fujita H, Jin J, Davis LS, Wang Y, Fogo AB, Breyer MD. Characterization of susceptibility of inbred mouse strains to diabetic nephropathy. *Diabetes* 54: 2628-37, 2005.
54. Qi ZH, I W, Mehta A, Jin JP, Zhao M, Harris RC, Fogo AB, Breyer MD. Serial determination of glomerular filtration rate in conscious mice using FITC-inulin clearance. *American Journal of Physiology-Renal Physiology* 286: F590-F596, 2004.
55. Robinson MD, McCarthy DJ, Smyth GK. edgeR: a Bioconductor package for differential expression analysis of digital gene expression data. *Bioinformatics* 26: 139-40, 2010.
56. Robinson MD, Smyth GK. Small-sample estimation of negative binomial dispersion, with applications to SAGE data. *Biostatistics* 9: 321-32, 2008.

57. Saleem MA, O'Hare MJ, Reiser J, Coward RJ, Inward CD, Farren T, Xing CY, Ni L, Mathieson PW, Mundel P. A conditionally immortalized human podocyte cell line demonstrating nephrin and podocin expression. *Journal of the American Society of Nephrology* 13: 630-8, 2002.
58. Samuel T, Hoy WE, Douglas-Denton R, Hughson MD, Bertram JF. Applicability of the glomerular size distribution coefficient in assessing human glomerular volume: the Weibel and Gomez method revisited. *J Anat* 210: 578-82, 2007.
59. Schörg A, Santambrogio S, Platt JL, Schödel J, Lindenmeyer MT, Cohen CD, Schrödter K, Mole DR, Wenger RH, Hoogewijs D. Destruction of a distal hypoxia response element abolishes trans-activation of the PAG1 gene mediated by HIF-independent chromatin looping. *Nucleic Acids Res* 43: 5810-23, 2015.
60. Singh S, Canseco DC, Manda SM, Shelton JM, Chirumamilla RR, Goetsch SC, Ye Q, Gerard RD, Schneider JW, Richardson JA, Rothermel BA, Mammen PP. Cytoglobin modulates myogenic progenitor cell viability and muscle regeneration. *Proc Natl Acad Sci U S A* 111: E129-38, 2014.
61. Stagner JI, Seelan RS, Parthasarathy RN, White K. Reduction of ischemic cell death in cultured Islets of Langerhans by the induction of cytoglobin. *Islets* 1: 50-4, 2009.
62. Storti F, Santambrogio S, Crowther LM, Otto T, Abreu-Rodriguez I, Kaufmann M, Hu CJ, Dame C, Fandrey J, Wenger RH, Hoogewijs D. A novel distal upstream hypoxia response element regulating oxygen-dependent erythropoietin gene expression. *Haematologica* 99: e45-8, 2014.
63. Susztak K, Raff AC, Schiffer M, Bottinger EP. Glucose-induced reactive oxygen species cause apoptosis of podocytes and podocyte depletion at the onset of diabetic nephropathy. *Diabetes* 55: 225-33, 2006.
64. Thuy le TT, Morita T, Yoshida K, Wakasa K, Iizuka M, Ogawa T, Mori M, Sekiya Y, Momen S, Motoyama H, Ikeda K, Yoshizato K, Kawada N. Promotion of liver and lung tumorigenesis in DEN-treated cytoglobin-deficient mice. *Am J Pathol* 179: 1050-60, 2011.
65. Thuy le TT, Van Thuy TT, Matsumoto Y, Hai H, Ikura Y, Yoshizato K, Kawada N. Absence of cytoglobin promotes multiple organ abnormalities in aged mice. *Sci Rep* 6: 24990, 2016.

66. Thuy LT, Matsumoto Y, Van Thuy TT, Hai H, Suoh M, Urahara Y, Motoyama H, Fujii H, Tamori A, Kubo S, Takemura S, Morita T, Yoshizato K, Kawada N. Cytoglobin Deficiency Promotes Liver Cancer Development from Hepatosteatosis through Activation of the Oxidative Stress Pathway. *Am J Pathol* 185: 1045-60, 2015.
67. Tian SF, Yang HH, Xiao DP, Huang YJ, He GY, Ma HR, Xia F, Shi XC. Mechanisms of neuroprotection from hypoxia-ischemia (HI) brain injury by up-regulation of cytoglobin (CYGB) in a neonatal rat model. *J Biol Chem* 288: 15988-6003, 2013.
68. Trandafir F, Hoogewijs D, Altieri F, Rivetti di Val Cervo P, Ramser K, Van Doorslaer S, Vanfleteren JR, Moens L, Dewilde S. Neuroglobin and cytoglobin as potential enzyme or substrate. *Gene* 398: 103-13, 2007.
69. Trent JT, 3rd, Hargrove MS. A ubiquitously expressed human hexacoordinate hemoglobin. *J Biol Chem* 277: 19538-45, 2002.
70. Tsachaki M, Birk J, Egert A, Odermatt A. Determination of the topology of endoplasmic reticulum membrane proteins using redox-sensitive green-fluorescence protein fusions. *Biochim Biophys Acta* 1853: 1672-82, 2015.
71. Tusher VG, Tibshirani R, Chu G. Significance analysis of microarrays applied to the ionizing radiation response. *Proc Natl Acad Sci U S A* 98: 5116-21, 2001.
72. Vinogradov SN, Moens L. Diversity of globin function: enzymatic, transport, storage, and sensing. *J Biol Chem* 283: 8773-7, 2008.
73. Wickham H. *ggplot2: Elegant Graphics for Data Analysis*: Springer-Verlag New York; 2016.
74. Xu R, Harrison PM, Chen M, Li L, Tsui TY, Fung PC, Cheung PT, Wang G, Li H, Diao Y, Krissansen GW, Xu S, Farzaneh F. Cytoglobin overexpression protects against damage-induced fibrosis. *Mol Ther* 13: 1093-100, 2006.
75. Yassin M, Kissow H, Vainer B, Joseph PD, Hay-Schmidt A, Olsen J, Pedersen AE. Cytoglobin affects tumorigenesis and the expression of ulcerative colitis-associated genes under chemically induced colitis in mice. *Sci Rep* 8: 6905, 2018.

Table 1: List of differentially expressed genes in shCYGB-1 compared to shCTR cells.

Genes are divided in four categories, anti-oxidant, podocyte phenotype, podocyte injury and apoptosis. P values are corrected for multiple statistical testing by FDR.

Function	Gene ID	Fold change	p-value
Anti-oxidant	<i>CYGB</i>	-28.92	1.1E-98
Anti-oxidant	<i>SOD3</i>	-3.70	8.0E-04
Anti-oxidant	<i>GPX3</i>	-4.69	9.97E-19
Anti-oxidant	<i>GPX7</i>	-2.96	4.8E-03
Anti-oxidant	<i>DUOX-1</i>	-18.14	3.3E-05
Anti-oxidant	<i>DUOX-2</i>	-12.40	3.8E-07
Podocyte phenotype	<i>MAFB</i>	-86.20	1.8E-25
Podocyte phenotype	<i>WT-1</i>	-2.26	4.1E-02
Podocyte injury	<i>SERPINE1</i>	2.19	1.87E-27
Apoptosis	<i>PYCARD</i>	-2.73	2.7E-06
Apoptosis	<i>TP73</i>	-2.45	2.05E-08

FIGURE LEGENDS

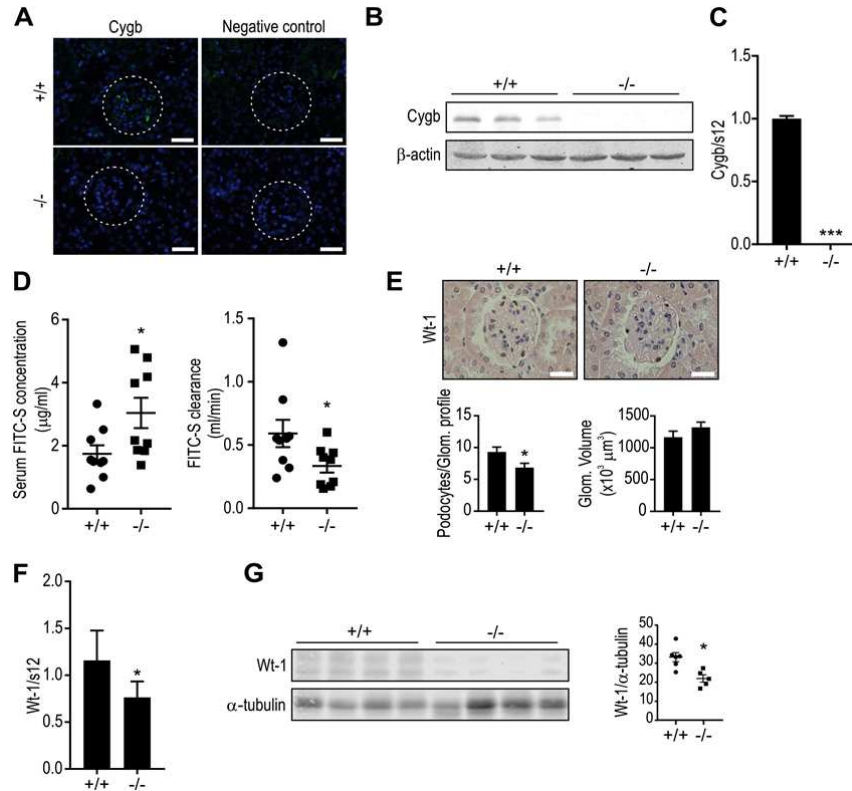


Fig.1 Cygb deficiency alters kidney function. **A.** Immunofluorescence detection of Cygb in WT (*Cygb*^{+/+}) and KO (*Cygb*^{-/-}) mice. Incubation without primary antibody served as negative control (scale bar 100 μM). Dashed white circle indicates glomerular region. Green: Cygb, blue: DAPI. **B.** RNA and **C.** protein levels of Cygb in *Cygb*^{+/+} and *Cygb*^{-/-} mice. β-actin was used as loading control. **D.** Serum FITC-sinistrin (FITC-S) concentration and clearance in *Cygb*^{+/+} and *Cygb*^{-/-} mice at baseline conditions. Results are indicated as mean ± SEM of n=9 for each group. *, p<0.05; Student's t-test. **E.** Wt-1 immunostaining in *Cygb*^{+/+} and *Cygb*^{-/-} mice (scale bar 20 μM). Average number of Wt-1-positive nuclei (bottom left) and average glomerular volume (bottom right) in the two groups. Results are indicated as mean ± SEM of n=5 mice for each group. Twenty glomeruli from each mouse were analyzed. *, p<0.05; Student's t-test. **F.** RNA and **G.** protein levels of Wt-1 with corresponding protein quantification. α-tubulin was used as loading control. *, p<0.05; Student's t-test.

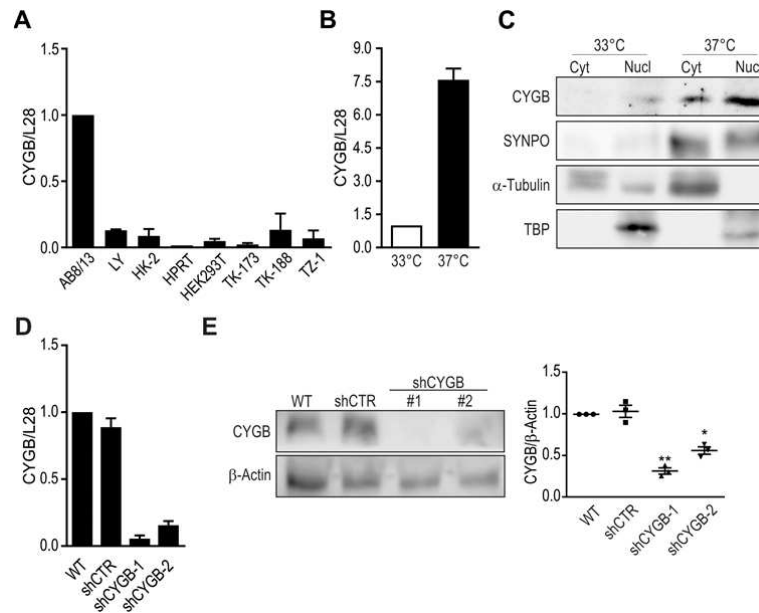


Fig.2 AB8/13 cells express abundant CYGB mRNA levels. A. CYGB mRNA expression in human kidney-derived cell lines. HK-2 and HPRT, proximal tubule cell lines; HEK293T, embryonic kidney; TK-173, TK-188 and TZ-1, fibroblasts; LY and AB8/13, podocytes (n=4) **B.** CYGB mRNA expression and **C.** CYGB protein levels in AB8/13 before (33°C) and after 10-14 days of differentiation at 37°C. Cyt, cytoplasmic fraction; Nucl, nuclear fraction. SYNPO was used as marker of differentiated podocytes, α -Tubulin as cytoplasmic marker and TBP as nuclear marker. **D.** Stable CYGB knock-down with two independent shRNA constructs (shCYGB-1, shCYGB-2) was confirmed on the mRNA level (n=4). ***, $p < 0.001$ compared to WT; one-way ANOVA and Tukey correction for multiple comparisons. **E.** Representative immunoblot (top panel) and densitometry analysis (bottom panel) of CYGB knock-down cells. β -Actin was used as loading control. *, $p < 0.05$; **, $p < 0.01$; compared to WT; one-way ANOVA and Tukey correction for multiple comparisons.

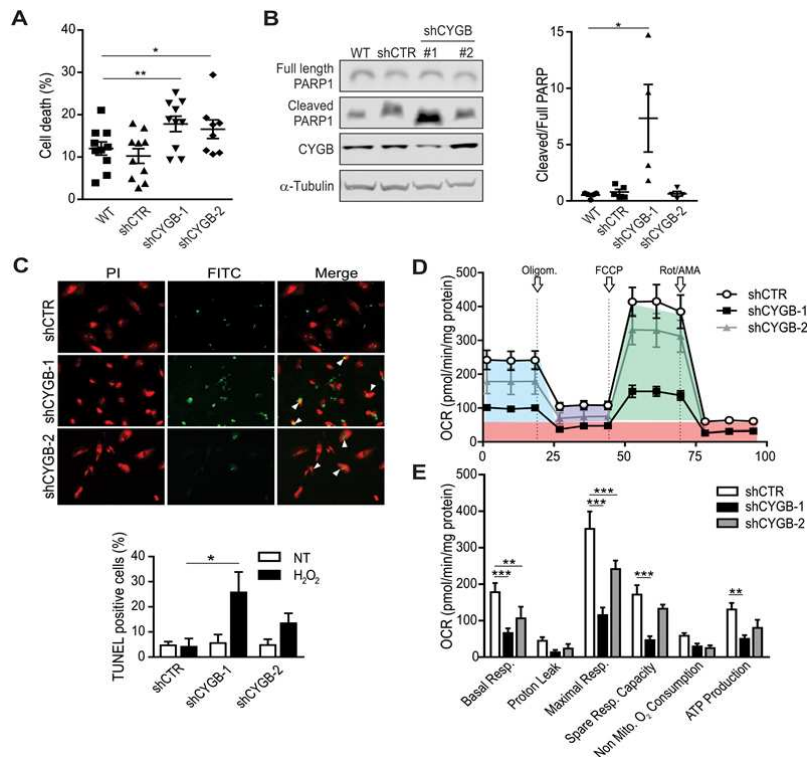


Fig.3 CYGB protects against cell death and apoptosis. **A.** Cell death was measured by trypan blue exclusion (n=8-10). **, $p < 0.01$; one-way ANOVA and Tukey correction for multiple comparisons. **B.** Representative immunoblot displaying PARP1 cleavage in CYGB knock-down cells compared to WT and shCTR (left panel) and densitometry analysis (right panel). α -Tubulin was used as loading control. **C.** TUNEL assay (FITC, Green) in shCTR, shCYGB-1 and shCYGB-2 cells following H_2O_2 treatment (top panel) and corresponding quantification of TUNEL-positive cells (bottom panel). PI, Propidium iodide. Arrowheads indicate TUNEL positive staining. *, $p < 0.05$; two-way ANOVA and Sidak's correction for multiple comparisons. **D.** OCR in shCTR, shCYGB-1 and shCYGB-2 cells with arrows indicating sequential injections into media of the specific stressors oligomycin (Oligom.), carbonyl cyanide-4 trifluoromethoxy phenylhydrazone (FCCP), and rotenone/antimycin A (Rot/AMA), normalized by protein content. Red, non-mitochondrial respiration; blue, basal respiration; purple, proton leak; green, maximal respiration. **E.** Comparison of different mitochondrial parameters calculated from the OCR profile in shCTR, shCYGB-1 and shCYGB-2 cells (n=4). ***, $p < 0.001$; **, $p < 0.01$; two-way ANOVA and Dunnett's multiple comparisons test.

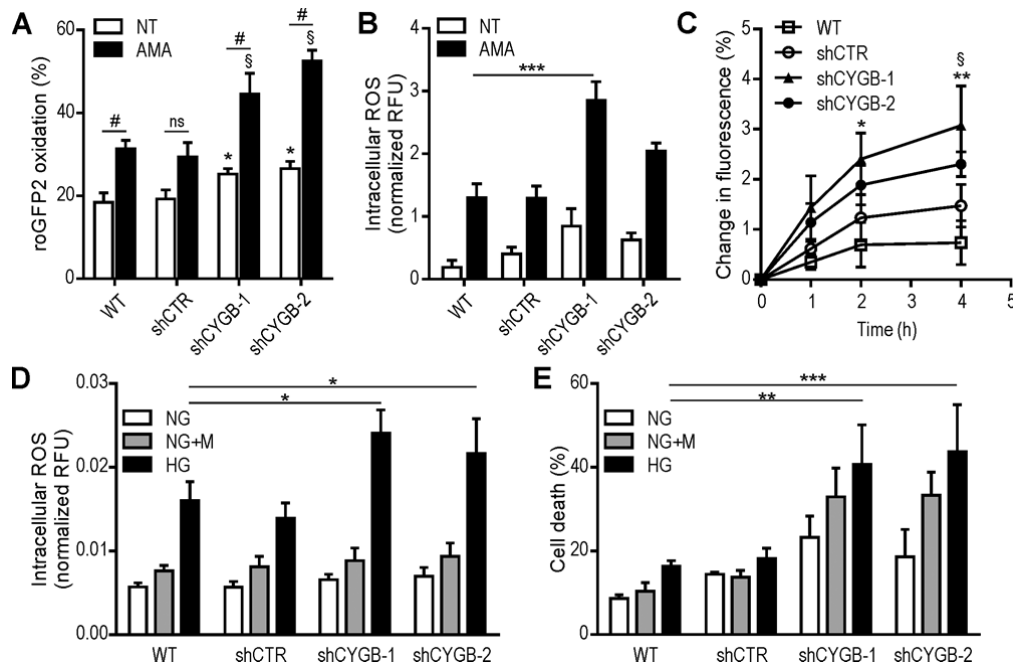


Fig.4 CYGB deficiency causes oxidative stress. **A.** Oxidation of the cytoplasmic redox-sensitive probe roGFP2-Orp1 in WT, shCTR, shCYGB-1 and shCYGB-2 cells under non-treated conditions (NT) and upon AMA treatment (n=4). *, p<0.05; Student's t test compared to NT WT cells; §, p<0.05; compared to AMA WT; #, p<0.001; ns, non-significant; two-way ANOVA and Tukey's post hoc test. **B.** Intracellular ROS production following AMA treatment (n=3). ***, p<0.001; two-way ANOVA and Tukey's post hoc test compared to WT and shCTR cells. **C.** Kinetics of H₂O₂ treatment in WT, shCTR, shCYGB-1 and shCYGB-2 cells *, p<0.05; **, p<0.01 (shCYGB-1 compared to WT); §, p<0.05 (shCYGB-2 compared to WT); two-way ANOVA and Tukey's post hoc test. (n=4-6). **D.** ROS accumulation in WT, shCTR and shCYGB-1 and shCYGB-2 cells upon normal (NG) or high (HG) glucose treatment. Mannitol (NG+M) was used as osmotic control (n=4). **E.** Cell death quantification (trypan blue exclusion method) of WT, shCTR and shCYGB-1 and shCYGB-2 cells subjected to normal (NG) or high (HG) glucose treatment. Mannitol (NG+M) was used as osmotic control (n=4). *, p<0.05; **, p<0.01; ***, p<0.001; two-way ANOVA and Tukey's post hoc test.

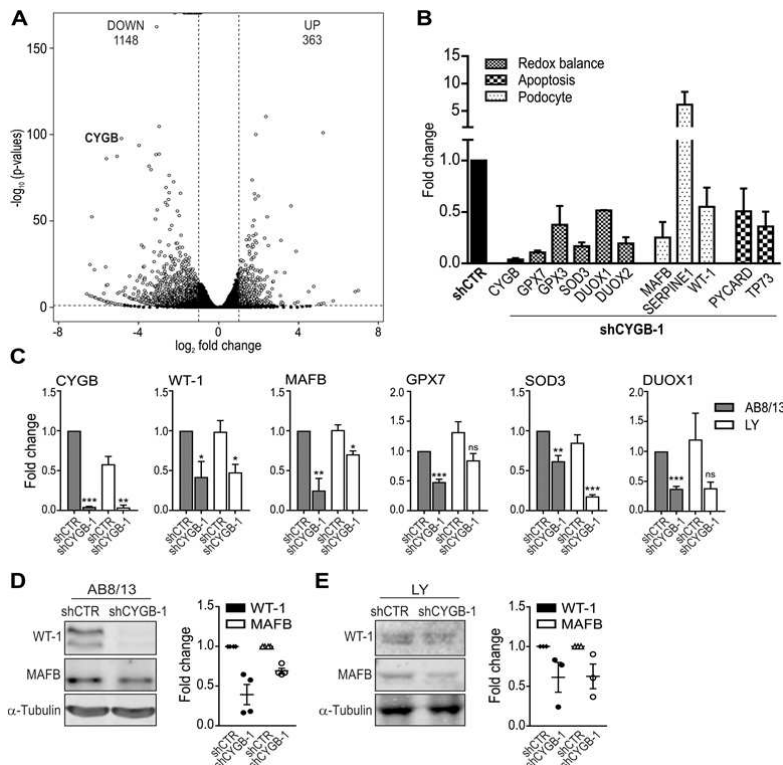


Fig.5 CYGB knock-down alters expression of genes involved in redox balance and podocyte phenotype maintenance. **A**. Volcano plot showing the distribution of differentially expressed genes following CYGB knock-down. White dots, |Fold change| > 2, $p < 0.05$; black dots, |Fold change| < 2, not significant. **B**. Validation of the results by RT-qPCR on independent RNA samples. **C**. Validation of selected genes downregulated in an independent podocyte cell line (LY), in comparison to AB8/13 ($n = 4$). *, $p < 0.05$; **, $p < 0.01$, ***, $p < 0.001$; Student's t-test. **D**, **E**. Representative immunoblot showing downregulation of two specific podocyte markers (MAFB and WT-1) in **D**. AB8/13 cells and **E**. in LY cells and corresponding quantification. α -Tubulin was used as loading control.

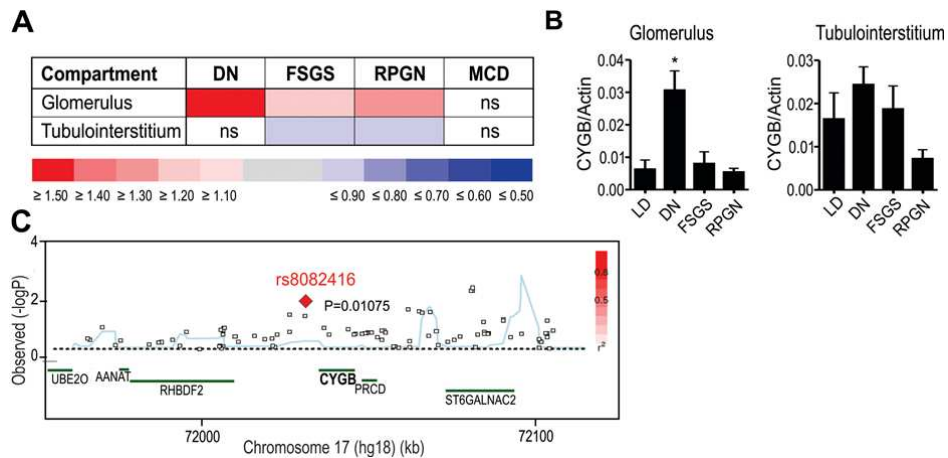
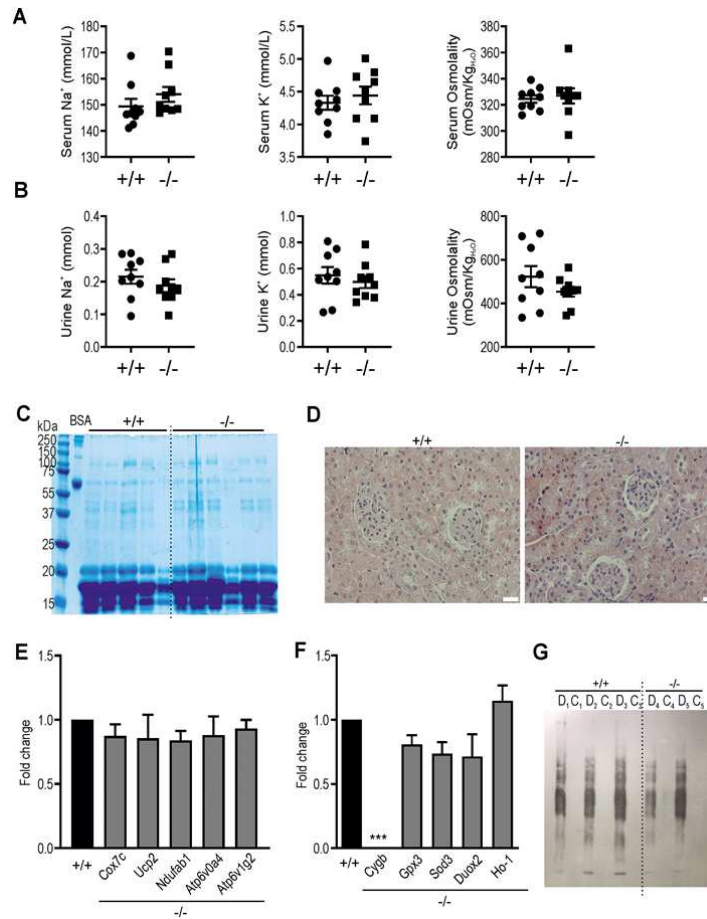


Fig.6. Association of *CYGB* with chronic kidney disease. **A.** Regional association plot for the *CYGB* gene region displaying a SNP associated with CKD obtained from a genome-wide association study (3). \log_{10} P values are plotted versus genomic position, using gene annotations obtained from the UCSC Genome Browser (RefSeq Genes, build 36). **B.** Gene expression data of microdissected glomeruli and tubulointerstitial compartments from patients with glomerulopathies. Values are Log fold changes relative to living donors (LD). DN, diabetic nephropathy; RPGN, rapidly progressive glomerulonephritis; FSGS, focal segmental glomerulosclerosis; MCD, minimal change disease. **C.** *CYGB* mRNA levels were validated in an independent cohort of microdissected samples by RT-PCR and normalized to β -Actin mRNA levels.

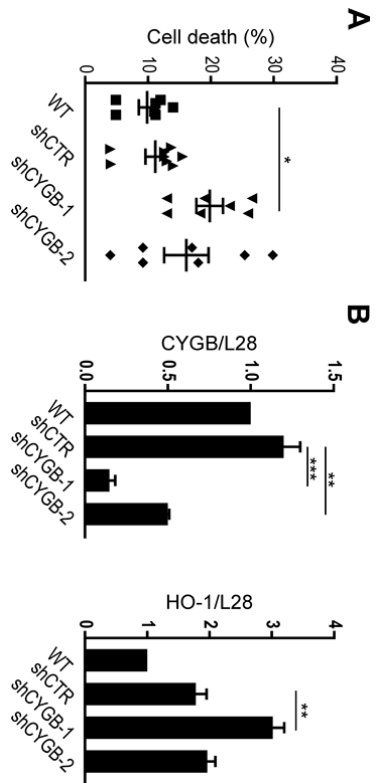


Supplem. Fig. S1 Effect of *Cygb* deficiency on serum and urine parameters. Na^+ , K^+ and osmolality were assessed for *Cygb*^{+/+} and *Cygb*^{-/-} mice in **A.** serum and **B.** urine samples. None of the analyzed parameters resulted in significant differences between the two groups. +/+, n=9; -/- n=9. **C.** Potential albuminuria assessment on *Cygb*^{+/+} and *Cygb*^{-/-} urine samples. BSA was used as positive control. **D.** Hematoxylin and eosin staining of *Cygb*^{+/+} and *Cygb*^{-/-} kidneys. **E.** RT-qPCR quantification of metabolism-related genes in whole kidney lysates of *Cygb*^{+/+} and *Cygb*^{-/-} mice. **F.** RT-qPCR quantification of *Cygb* and anti-oxidative genes in *Cygb*^{+/+} and *Cygb*^{-/-} mice. ***, p<0.001; one-way ANOVA and Tukey's post hoc test. **G.** OxyBlot on *Cygb*^{+/+} and *Cygb*^{-/-} mice. Derivatization-treated (D) and negative control (C) from the same specimen are displayed with the same number. *Cygb*^{+/+}, n=3; *Cygb*^{-/-} n=2.

Antioxidants and Redox Signaling

The anti-oxidative role of cytoglobin in podocytes: implications for a role in chronic kidney disease. (DOI: 10.1089/ars.2019.7868)

This paper has been peer-reviewed and accepted for publication, but has yet to undergo copyediting and proof correction. The final published version may differ from this proof.



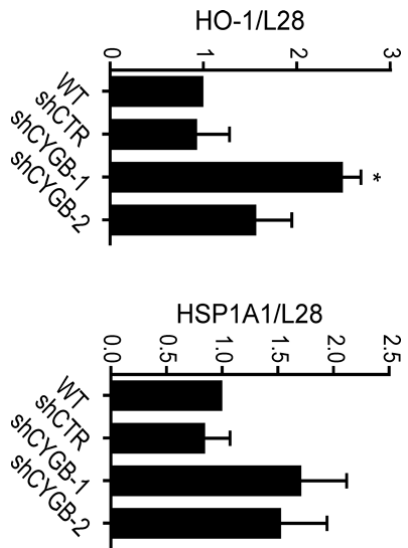
42

Supplem. Fig. S2 CYGB knock-down in the podocyte cell line LY. A. Cell death was measured by trypan blue exclusion (n=6-8). *, $p < 0.05$; one-way ANOVA and Tukey correction for multiple comparisons. **B.** RT-qPCR quantification of CYGB and HO-1 in WT, shCTR, shCYGB-1 and shCYGB-2 cells (n=4). **, $p < 0.01$; ***, $p < 0.001$; one-way ANOVA and Tukey's post hoc test.

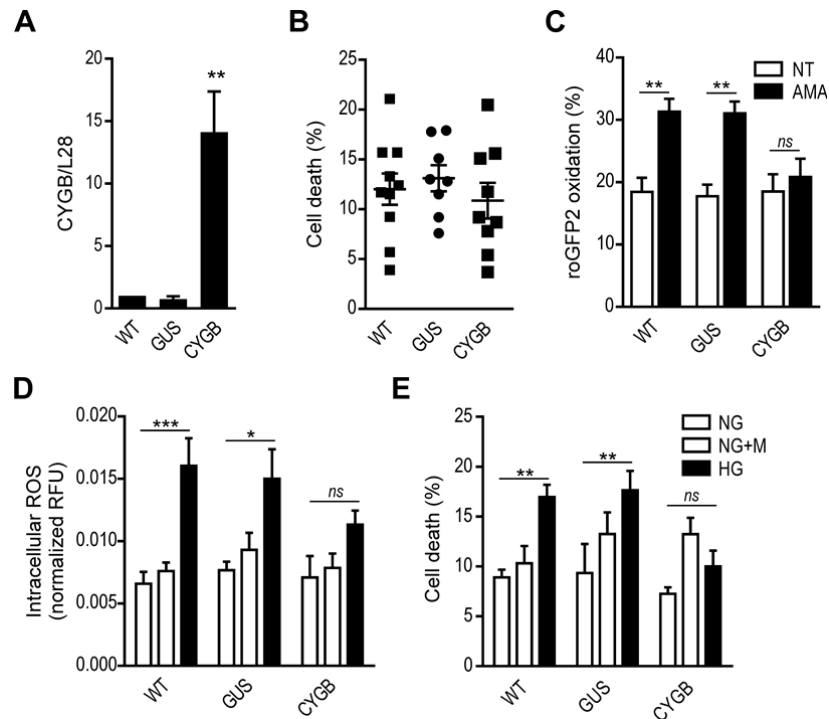
Antioxidants and Redox Signaling

The anti-oxidative role of cytoglobin in podocytes: implications for a role in chronic kidney disease. (DOI: 10.1089/ars.2019.7868)

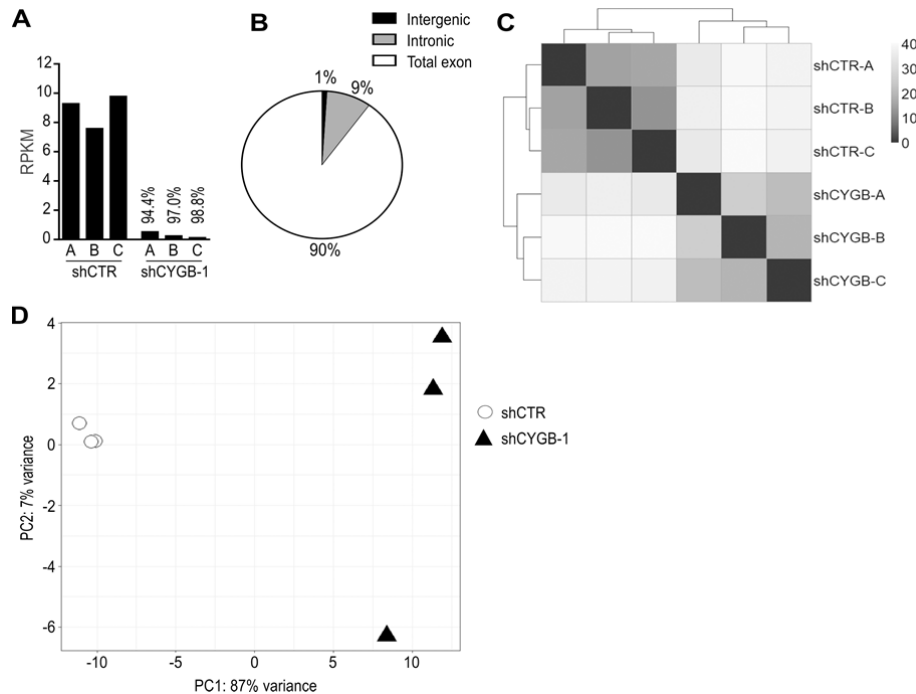
This paper has been peer-reviewed and accepted for publication, but has yet to undergo copyediting and proof correction. The final published version may differ from this proof.



Supplem. Fig. S3 Transcript levels of the anti-oxidant genes *HO-1* and *HSP1A1* measured by RT-qPCR in WT, shCTR, shCYGB-1 and shCYGB-2 AB8/13 cells (n=4). *, p<0.05; Student's t-test.



Supplem. Fig. S4 CYGB overexpression protects podocytes against ROS accumulation and cell death. **A.** Efficacy of CYGB overexpression in AB8/13 cells (n=4). **, p<0.01; Student's t test. **B.** Cell death measured by trypan blue exclusion. **C.** Quantification of roGFP2 oxidation in non-treated (NT) and antimycin A (AMA) treated cells (n=4).*, p<0.05; ns, not significant; two-way ANOVA and Tukey correction for multiple comparisons. **D.** Measurement of intracellular ROS accumulation by H2DCFDA fluorescence (n=4). ***, p<0.001; *, p<0.05; ns, not significant; two-way ANOVA and Tukey correction for multiple comparisons. **E.** Corresponding cell death upon normal (NG) or high (HG) glucose treatment. Mannitol (NG+M) served as osmotic control. GUS (β -glucuronidase) overexpression was used as negative control for CYGB overexpression (n=4). **, p<0.01; ns, not significant; two-way ANOVA and Dunnett's correction for multiple comparisons.

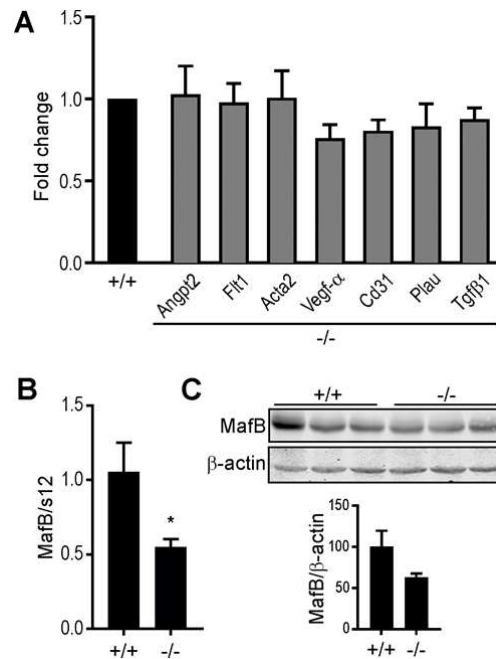


Supplem. Fig. S5 Expanded RNA-sequencing data. **A.** CYGB transcript levels in RPKM (Reads Per Kilobase per Million mapped reads) of multiple mapping in transcriptome analysis of WT and CYGB knock-down AB8/13 podocytes. **B.** Mapping reads classification into total exons, introns and intergenic regions. **C.** Sample-to-sample distance and **D** principal component analysis (PCA) of the RNA-sequencing datasets indicate clear separation among shCYGB and shCTR cells.

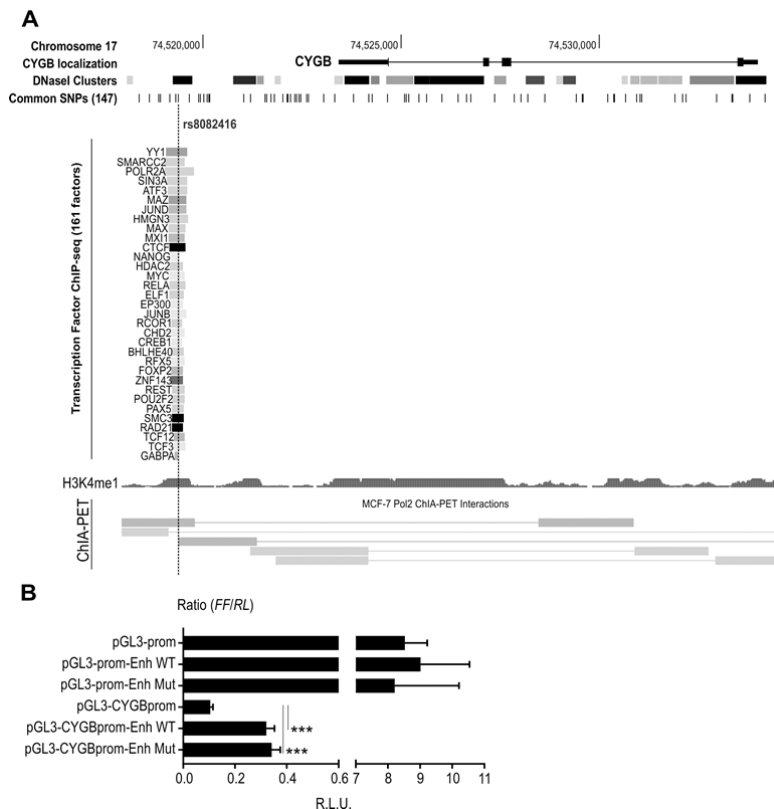
This paper has been peer-reviewed and accepted for publication, but has yet to undergo copyediting and proof correction. The final published version may differ from this proof.

Antioxidants and Redox Signaling

The anti-oxidative role of cytoglobin in podocytes: implications for a role in chronic kidney disease. (DOI: 10.1089/ars.2019.7868)



Supplem. Fig. S6 Marker gene and MafB expression in mice. **A.** RT-qPCR quantification of fibrosis and vasculature marker genes in *Cygb*^{+/+} and *Cygb*^{-/-} mice. **B.** mRNA and **C.** protein levels of MafB in *Cygb*^{+/+} and *Cygb*^{-/-} mice and corresponding immunoblot quantification. β -actin was used as loading control. *, $p < 0.05$; Student's t-test. Abbreviations: Angpt2, Angiotensin-2; Flt1, Vascular endothelial growth factor receptor 1; Acta2, α -smooth muscle actin; Vegf- α , Vascular endothelial growth factor A; Cd31, cluster of differentiation 31 (also known as Pecam, Platelet endothelial cell adhesion molecule); Plau, Plasminogen Activator Urokinase; Tgfb β 1, Transforming growth factor beta 1.

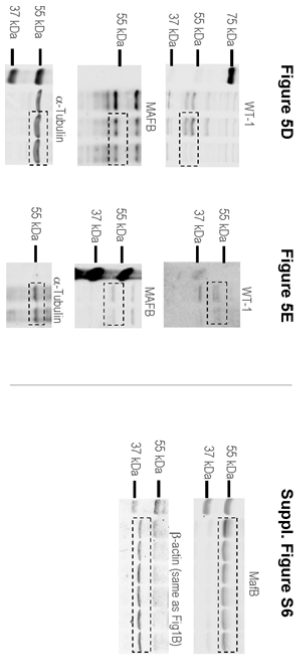
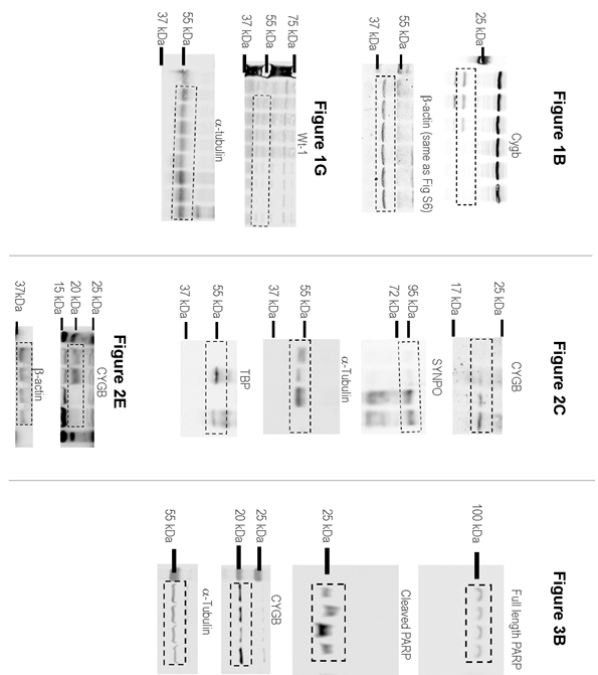


Supplem. Fig. S7 SNP rs8082416 coincides with a DNaseI hypersensitivity cluster and strong transcription factor occupancy. **A.** UCSC Genome Browser output (*hg19*) of SNP rs8082416 and the *CYGB* gene locus illustrating that the SNP is located in the 3' intergenic region of *CYGB* and localized in a DNaseI hypersensitivity cluster with substantial transcription factor occupancy. Gray saturation is proportional to the maximum signal strength observed in any cell line. Additionally, ChIA-PET interaction studies suggest loop formation between the SNP area and the first intron close to transcription initiation region of the *CYGB* gene. **B.** SV40 promoter (pGL3-prom) and *CYGB* promoter (*CYGB*prom) driven firefly luciferase reporter genes were transiently cotransfected into HEK293T cells. An enhancer fragment of 90 bp spanning the WT SNP rs8082416 (Enh WT) or mutated SNP (Enh Mut) was added to the SV40 promoter and *CYGB* promoter-driven firefly luciferase reporter genes. Results are displayed as ratios of firefly to *Renilla* luciferase activities in relative light units (R.L.U.) from three independent experiments performed in triplicates, error bars correspond to the SEM. ***, $p < 0.001$; Student's t-test.

Antioxidants and Redox Signaling

The anti-oxidative role of cytoglobin in podocytes: implications for a role in chronic kidney disease. (DOI: 10.1089/ars.2019.7868)

This paper has been peer-reviewed and accepted for publication, but has yet to undergo copyediting and proof correction. The final published version may differ from this proof.



Suppl. Fig. S8 Original versions of immunoblots shown in Figure 1, 2, 3, 5 and S6.

Antioxidants and Redox Signaling

The anti-oxidative role of cytoglobin in podocytes: implications for a role in chronic kidney disease. (DOI: 10.1089/ars.2019.7868)

This paper has been peer-reviewed and accepted for publication, but has yet to undergo copyediting and proof correction. The final published version may differ from this proof.

Supplementary Table 1. Primers used for RT-qPCR quantification

mRNA	Forward primer (5'-3')	Reverse primer (5'-3')	Amplico size (bp)
<i>CYGB</i>	CAAGGTGGAACCGGTACT	TCACGTGGCTGTAGATGAGG	137
<i>DUOX1</i>	CAGCTGAAAAGAGAAAACAAAG	TGCAGAGTGTGTTCTTAGGC	138
<i>DUOX2</i>	GAAGGCTGTGACAAAAGCAGC	AACATGTCCCTGGGGCTTGAG	201
<i>GPX3</i>	AACTCCTGTCTCCACCCTC	ATCTGACGTTGCTGAACCGT	167
<i>GPX7</i>	GCAGGAGCAGGACTCTACG	CTCGGTAGTGTGCTGTGTG	137
<i>HO-1</i>	ATGACACCAAGGACCAGAGC	GTGTAAGGACCCATCGGAGA	153
<i>HSP1A1</i>	TGCTGATCCAGGTGTACGAG	CGTTGGTGAATGTGATCTTG	204
<i>L28</i>	GCAATTCCTCCGCTACAAAC	TGTTCTTGGGGATCATGTGT	198
<i>MAFB</i>	TGACCTGCTCAAGTTTCGAC	AGTTGCTCGCCATCCAGTAC	204
<i>PYCARD</i>	GCCGAGGAGCTCAAGAAAGTT	ATAAAGTGCAGGCCCTGGCCTT	296
<i>SERPINE1</i>	GACCTCAGGAAGCCCTTAGA	ACTGTTCTGTGGGGTTGTG	275
<i>SOD3</i>	CGAGACATGTACGCCAAAGT	AACTGATGCACGTGGATGG	248
<i>TP73</i>	CGAAATGCCCAACAAACGGC	AGATTGAACTGGGCCGTGG	247
<i>WT-1</i>	GCGGAGCCCAATACAGAAATA	TCTCACCAGTGTGCTTCCTG	207
<i>Ogb</i>	CCATCCTGGTGAAGTTCCTTGT	GATCCTCCATGTGTCTAACTG	75
<i>Wt-1</i>	GCCTTCACC TTGCACCTTCTC	GACCGTGTGTATCTCTTGGT	186
<i>MafB</i>	TGTTGTTCAAGTCCCTTCCG	TCCTCTTACTGAACCCGCGA	95
<i>s12</i>	GAAAGCTGCCAAAAGCCTTAGA	AACTGCAACCAACCCCTTC	214
<i>Ahp6/1g2</i>	AGTGAAAACGGGAGCCGTAA	GCCCTTCCTTCCCTGGCATC	222
<i>Cox7c</i>	AGGGTCCGGGGAAAGAAATTG	AAAAGAAAAGTGGGGCAAAAC	101
<i>Ahp6/0a4</i>	AGGCTGCCGTATTGCTGTGTA	TAGAGTCGTCTCCAGGGTGTAT	242
<i>Ucp2</i>	GCGGTCCGGACACAAATAGTA	GGGACCTTCAATCGGCAAGA	216
<i>Ndufab1</i>	TGGAAGACGAATTTGGGTTTGA	TGGCAATGACCAAGAGAAAGTGGA	140
<i>Angr12</i>	GCACAAAAGGATTCGGACAAAT	AASTTGGAAAGACCACATGC	94
<i>Fli1</i>	TGAGGAGCTTTCCACCGAACT	TATCTTCATGGAAGCCCTTGG	130
<i>Tgf-β1</i>	GAGCCCGAAGCCGGACTACT	TTGGGGTCCACCATTAGCA	59
<i>Aclaz</i>	TCCTGAGAGAAAGAGCTAACGAACT	AAAGGTTTCGTTTCCAAATGGT	62
<i>Vegfa</i>	CAGGCTGCTGTAAACGATGAA	GCATTCACATCTGCTGTGCT	140
<i>Pecam1 (Cd31)</i>	AAACAGAAAACCCGTGGAGATG	GGCTTCCACACTAGGCTCAG	86
<i>Plau</i>	CCTACAAATGCCACAGACCT	CAAACCTGCCCTTAGGCCAATC	120

Antioxidants and Redox Signaling

The anti-oxidative role of cytoglobin in podocytes: implications for a role in chronic kidney disease. (DOI: 10.1089/ars.2019.7868)

This paper has been peer-reviewed and accepted for publication, but has yet to undergo copyediting and proof correction. The final published version may differ from this proof.

Supplementary Table 2. Details of RNA-sequencing mapping statistics.

50

Sample	# of raw reads	# of pre-processed reads	% pre-processed reads	# of mapped reads	% mapped reads	% reads mapped to exon region	% reads mapped to intronic region	% reads mapped to intergenic region
shCTR-A	30,153,616	26,976,062	89.46	25,777,431	95.56	89.8	8.9	1.3
shCTR-B	29,171,024	26,084,110	89.42	24,885,595	95.41	89.41	9.22	1.37
shCTR-C	28,754,530	25,656,745	89.23	24,522,454	95.58	90.53	8.19	1.28
shCYGB-A	27,097,202	24,260,728	89.53	23,267,165	95.90	90.8	8.02	1.18
shCYGB-B	28,167,338	25,193,444	89.44	24,351,185	96.66	90.08	8.75	1.16
shCYGB-C	26,183,974	23,419,816	89.44	22,439,161	95.81	88.91	9.85	1.24

Antioxidants and Redox Signaling

The anti-oxidative role of cytoglobin in podocytes: implications for a role in chronic kidney disease. (DOI: 10.1089/ars.2019.7868)

This paper has been peer-reviewed and accepted for publication, but has yet to undergo copyediting and proof correction. The final published version may differ from this proof.

Supplementary Table 3. Literature-based podocyte marker set. FC, Fold Change; FDR, False Discovery Rate; RPKM, Reads Per Kilobase Million mapped reads; SD, Standard Deviation

GENE	FC	FDR	shCTR_RPKM	shCTR_SD	shCYGB_RPKM	shCYGB_SD
ACTN4	1.09	1.00E+00	159.22	11.48	166.92	23.79
AKT2	-1.07	1.00E+00	7.23	0.2	6.45	0.73
ARRHGDA	1.27	2.70E-01	66.36	6.83	80.85	18.31
ATG5	1.19	2.37E-01	11.2	0.53	12.78	0.66
ATG7	-1.17	5.94E-01	4.85	0.2	3.96	0.53
ATP6AP2	1.2	7.48E-02	80.92	3.45	93.23	2.54
BRAF	1.17	4.53E-01	2.52	0.12	2.82	0.07
CD151	-1.14	5.44E-01	104.79	2.8	87.87	9.59
CD2AP	1.66	1.04E-09	20.69	1.19	32.95	2.08
CD2BP2	-1.07	1.00E+00	19.4	0.91	17.37	1.53
CD55	-1.27	5.79E-02	6.88	0.27	5.19	0.4
CDC42	1.18	2.50E-01	83.13	2.14	94.14	9.13
CEBPA	1.24	1.00E+00	0.11	0.02	0.13	0.03
CFL1	1.2	1.35E-01	172.92	11.17	198.25	16.25
CLIC5	1.92	1.00E+00	0	0.01	0.01	0.01
COL4A3	1.02	1.00E+00	0.03	0.02	0.03	0.01
CTSD	1.17	8.47E-01	93.03	11.25	104.49	19.63
DNM1	-1.12	1.00E+00	5.62	0.36	4.82	1.2
ENPEP	-1.97	9.49E-03	2.14	0.41	1.03	0.43
EXT1	1.3	4.86E-03	23.89	1.41	29.68	1.07
EZR	1.36	1.28E-04	109.15	7.08	142.4	4.14
FAT1	-1.08	1.00E+00	31.47	3.39	27.86	1.85
FLT1	-5.84	8.88E-03	0.05	0.02	0.01	0
FOXC1	1.02	1.00E+00	7.59	1.18	7.46	0.91
FOXC2	1.44	3.21E-02	3.26	0.58	4.48	0.43
FVN	1.26	4.38E-02	6.04	0.29	7.26	0.24
IGF1R	1.24	2.29E-01	6.87	1.22	8.18	0.19
INSR	1.04	1.00E+00	0.05	0.01	0.05	0.02
ITGB1	1.13	7.68E-01	446.48	13.27	481.88	48.65
KANK1	1.39	4.95E-04	2.72	0.14	3.64	0.11
KIRREL	-1.1	1.00E+00	52.01	2.8	45.27	5.09
KLF4	1.28	1.00E+00	0.67	0.22	0.82	0.07
KLF6	1.35	2.91E-04	22.27	0.89	28.86	0.86
LAMA5	-1.95	6.51E-03	4.96	0.98	2.45	1.11
LMX1B	-10.99	8.95E-01	0.02	0.02	0	0
MAFB	-86.2	1.78E-25	1.05	0.24	0.01	0.01
MAAG2	-1.58	7.90E-02	0.37	0.01	0.23	0.04
MDM2	-1.55	2.63E-09	81.88	3.62	50.51	2.02
MIET	-1.25	4.30E-02	44.95	2.39	34.36	3.16
MPP5	1.39	3.85E-04	6.52	0.45	8.69	0.33
MTOR	1.07	1.00E+00	7.6	0.06	7.77	0.29

Antioxidants and Redox Signaling

The anti-oxidative role of cytoglobin in podocytes: implications for a role in chronic kidney disease. (DOI: 10.1089/ars.2019.7868)

This paper has been peer-reviewed and accepted for publication, but has yet to undergo copyediting and proof correction. The final published version may differ from this proof.

MYH9	1.32	1.53E+03	288.2	16.59	363.77	22.93
MYOIE	1.07	1.00E+00	21.87	1.43	22.33	0.88
NCK2	-1.34	2.28E-02	14.24	1	10.2	1.42
NDST1	1.42	2.48E-04	68.5	4.27	92.66	8.48
NPHS1	-2.85	1.00E+00	0.02	0.02	0.01	0.01
NPHS2	1	1.00E+00	0	0	0	0
NR2C2	1.03	1.00E+00	5.21	0.31	5.12	0.14
NRP1	-2.2	0.00E+00	32.87	0.26	14.29	2.22
OOG	1.27	2.03E-01	12.23	0.95	14.88	2.96
PSSS2	1.2	6.00E-01	2.81	0.06	3.23	0.37
PHB2	1.01	1.00E+00	43.5	0.94	42.14	0.27
PIK3C3	1.39	3.48E-04	3.58	0.19	4.76	0.13
PIK3R1	-1.34	3.56E-02	4.99	0.27	3.57	0.54
PIK3R2	1.43	1.02E-01	4.49	0.36	6.14	1.68
PLCE1	1.37	8.10E-03	2.29	0.22	2.99	0.23
PODXL	-3.68	1.74E-42	5.22	0.26	1.36	0.1
PPARG	3.65	5.10E-07	0.19	0.11	0.66	0.07
PRKCI	-1.05	1.00E+00	21.32	0.63	19.35	1.7
PTEN	-1.08	1.00E+00	7.75	0.4	6.87	0.11
PTPRO	-1.09	1.00E+00	0.05	0.01	0.05	0.02
RAC1	1.06	1.00E+00	96.66	2.33	97.68	3.94
RET	-6.72	2.48E-01	0.04	0.01	0	0.01
RHOA	1.06	1.00E+00	232.67	7.21	235.36	19.36
RHPN1	-1.21	1.00E+00	1.38	0.21	1.1	0.53
RICTOR	1.19	6.81E-01	3.6	0.22	4.09	0.69
ROBO2	1.6	1.00E+00	0	0	0.01	0.01
SCHIP1	-2.03	1.00E+00	0.21	0.12	0.1	0.14
SDC4	1.09	1.00E+00	433.89	32.22	455.05	89.71
SIRT1	-1.2	1.98E-01	7.84	0.24	6.26	0.18
SYNPO	-1.69	4.55E-04	2.91	0.55	1.65	0.25
TOF21	-1.69	2.24E-02	0.98	0.19	0.55	0.07
TJP1	1.13	6.65E-01	13.21	0.5	14.25	0.54
TLN1	1.24	2.24E-02	85.49	2.31	101.19	6.92
TSC1	1.37	1.68E-02	4.14	0.09	5.43	0.85
VANGL2	-1.19	3.11E-01	14.19	1.34	11.39	0.68
VEGFA	-1.46	8.62E-04	14.93	2.38	9.79	0.79
VHL	1.06	1.00E+00	11.83	0.64	12	1.11
WASL	1.14	6.38E-01	13.74	0.42	14.66	0.88
WT-1	-2.26	4.12E-02	0.97	0.13	0.41	0.35
XBP1	1.19	1.74E-01	23.22	0.55	26.37	0.52
YAP1	-1.23	3.31E-02	44.47	1.12	34.75	1.78

Supplementary Table 4. Single cell RNA-sequencing based podocyte marker set. FC, Fold Change; FDR, False Discovery Rate; RPKM, Reads Per Kilobase Million mapped reads; SD, Standard Deviation

GENE	FC	FDR	shCTR_RPKM	shCTR_SD	shCYGB_RPKM	shCYGB_SD
MT-ATP8	-1.05	1.00E+00	1365.92	119.72	1239.86	204.57
SDC4	1.09	1.00E+00	433.89	32.22	455.05	89.71
EZR	1.36	1.28E-04	109.15	7.08	142.40	4.14
CD59	1.24	5.99E-02	102.46	11.27	121.81	5.11
ARPC1A	-1.09	1.00E+00	68.31	6.55	60.28	3.47
HLA-A	1.41	1.11E-04	65.60	5.74	88.83	3.83
ALCAM	1.26	2.30E-02	48.37	1.89	58.48	5.10
ITGAV	1.79	8.44E-10	46.65	1.04	79.89	11.17
GPC1	-1.48	4.72E-02	46.33	4.12	30.13	9.74
GADD45A	-1.28	8.12E-03	44.29	0.55	33.05	1.07
ITGB5	-1.12	9.30E-01	35.92	1.87	30.82	2.05
CRYAB	1.37	3.69E-01	30.72	6.67	40.08	12.10
SEPT10	-1.01	1.00E+00	27.78	2.30	26.45	1.90
AIF1L	1.12	1.00E+00	25.14	0.53	27.00	3.26
RAB38	1.65	2.04E-09	23.69	0.21	37.25	3.56
DPPI4	-1.46	6.45E-03	22.70	1.37	14.93	3.56
NSF	1.43	4.25E-05	20.85	0.64	28.50	2.23
PARVA	1.32	1.62E-03	18.31	0.89	23.09	1.01
TMO03	1.13	7.06E-01	17.49	1.23	18.92	0.77
GOLIM4	-1.24	7.62E-02	17.04	1.31	13.19	0.54
LGR4	-1.74	7.54E-10	16.98	1.16	9.35	1.02
AOX1	-1.17	1.00E+00	16.52	3.94	13.50	1.55
TSC22D1	-1.11	8.75E-01	16.41	0.34	14.18	0.51
FNBP1L	1.07	1.00E+00	16.12	1.49	16.44	2.17
VEGFA	-1.46	8.62E-04	14.93	2.38	9.79	0.79
ANXA4	1.06	1.00E+00	14.18	0.54	14.35	1.80
PAK1	1.11	8.95E-01	13.27	0.52	14.12	0.03
FGFR1	-1.30	1.61E-02	11.41	0.58	8.44	0.95
LPIN2	1.09	1.00E+00	10.94	0.27	11.47	0.45
CERS6	-1.04	1.00E+00	10.81	0.78	9.96	1.06
DNAJC11	1.15	5.46E-01	9.08	0.35	9.97	0.35
MOC52	1.02	1.00E+00	8.18	1.03	7.97	1.34
ILDR2	1.16	7.28E-01	8.11	0.52	8.99	1.19
CTSV	-2.26	3.45E-14	7.83	0.64	3.33	0.54
MPP5	1.39	3.85E-04	6.52	0.45	8.69	0.33
ARHGEF18	1.45	4.60E-03	6.11	0.91	8.49	1.01
IFT80	-1.18	6.19E-01	5.78	0.50	4.70	0.51
PODXL	-3.68	1.74E-42	5.22	0.26	1.36	0.10
MTSS1	1.03	1.00E+00	4.91	0.71	4.85	0.45
CDKN1C	-2.47	3.74E-06	4.65	1.38	1.81	0.42
HAUS8	-1.27	1.73E-01	4.65	0.50	3.51	0.18

Antioxidants and Redox Signaling

The anti-oxidative role of cytoglobin in podocytes: implications for a role in chronic kidney disease. (DOI: 10.1089/ars.2019.7868)

This paper has been peer-reviewed and accepted for publication, but has yet to undergo copyediting and proof correction. The final published version may differ from this proof.

Antioxidants and Redox Signaling

The anti-oxidative role of cytoglobin in podocytes: implications for a role in chronic kidney disease. (DOI: 10.1089/ars.2019.7868)

This paper has been peer-reviewed and accepted for publication, but has yet to undergo copyediting and proof correction. The final published version may differ from this proof.

Supplementary Table 5. Altered pathways related to renal disease, based on Ingenuity Pathway Analysis. (B-H=Benjamini-Hochberg)

54

Category	B-H; p-value	Molecules
Glomerular Injury	4.66E-02; 6.2E-01	WT-1, CDKN1G, SDFN, ANLN, DCN, CDKN2C, SALL1, BUB1B, KCP, PDGFB, CTSV, BDKRB2, CAAC4B, SCGB1A1, CAMK2A, CCL2, EDN1, WFDC2, RARB, LAMA1, ITGB4, SERPINE1, BDKRB1
Kidney Failure	2.44E-03; 3.89E-01	CACGNAT5, GDNF, PDE4A, AGHE, CAAC4B, AR, EDN1, TOP2A, CDH16, SERPINE1, GABRD, PDE11A, PPARG, GSTM1, WT-1, CACGNATD, GUCY1A3, FLT1, PDE4C, DCN, PTGS1, DRD2, BUB1B, KOPG, ABRE, NPPB, ITGAM, LDLR, NPR3, WFDC2, NPR1, SLC6A4, HMGCR
Renal Necrosis / Cell Death	8.23E-02; 1E00	GAS7, MAP2K6, TGF4, SLC22A3, CTGF, PYCARD, TP73, IL32, EMP2, UNC5B, TMEFF2, PSEN2, NTN1, AR, EDN1, FGF14, MCOLN3, MAP1LC3A, SLC22A2, RASSF5, PPARG, WT-1, APOBEC3B, NLRP3, FLT1, DCN, SALL1, LRRK2, IER3, TTPR1, IL24, BIRC5, CDK1, AREG, CCNB1, STRA6, PTH1R, IGFBP3, MAP3K8, MAFB, SFRP1, P2RX7, SLC47A1, RBP4
Nephrosis	1.74E-01; 1E00	CA2, SLC12A3, EMP2, PDE4A
Renal Degeneration	1.74E-01; 2.86E-01	COB, CLDN16, HSD17B2
Renal Proliferation	1.74E-01; 4.28E-01	DLGAP5, GDMRN, UNC5B, GDF9, TMEFF2, PLK1, CODC8, AURKA, BIRC5, PDGFB, NTN1, FGF13, PTGES, IGF2, EDN1, APLN, STEAP2, FGF14, CDC45, FBLN2, P2RX7, CEACAM1, OXTR
Renal Fibrosis	1.74E-01; 2.09E-01	BDKRB2, WT-1, CCL2, GDNF, WFDC2, DCN, BUB1B, BDKRB1, KCP
Renal Hydronephrosis	1.46E-01; 1.48E-01	SFRP2, MMP3, CCL2, DCN, NFYA, RARB, TGFBR2, IMPA2, ITGB4, HSPA4L, TNFRSF11B
Renal Damage	9.8E-02; 5.95E-01	GSTM1, UNC5B, LRRK2, IGFBP5, CP, SLC38A3, NTN1, CAAC4B, BDKRB2, PREX1, CAMK2A, EDN1, IGFBP3, HCK, TLR3, SLC22A2, ALOX5, SERPINE1, ITGB6, CRYM, C3AR1, BDKRB1, GJB2
Renal Atrophy	1.74E-01; 5.43E-01	DCN, SALL1, LRRK2, EFEMP1, BUB1B, HSPA4L
Renal Degradation	2.43E-01; 2.43E-01	LAMA1
Renal Inflammation	2.43E-01; 1E00	WT-1, SOCS1, TGF4, GDNF, DCN, IL21R, PTGS1, LRRK2, PSEN2, GPX7, CAAC4B, SLC19A3, ITGAM, CCL2, TOP2A, TLR3, RASSF5, SERPINE1
Renal Nephritis	2.43E-01; 1E00	WT-1, SOCS1, TGF4, GDNF, DCN, IL21R, PTGS1, LRRK2, PSEN2, GPX7, CAAC4B, SLC19A3, ITGAM, CCL2, TOP2A, TLR3, RASSF5, SERPINE1
Renal Cellular Infiltration	3.02E-01; 3.02E-01	LTB
Renal Hypoplasia	3.02E-01; 5.07E-01	RARB, PBX1, SALL1, PDGFB
Renal Dysfunction	3.11E-01; 3.11E-01	HPSE, VWF, ALOX5
Renal Tubule Injury	3.51E-01; 5.95E-01	GSTM1, EDN1, IGFBP3, IGFBP5, CP, SLC22A2, SERPINE1, CRYM, GJB2, SLC38A3
Renal Hypertrophy	4.14E-01; 6.2E-01	EDN1, GDNF, RARB, HSD17B2
Increased Levels of Albumin	4.19E-01; 4.19E-01	P2RX7
Renal Transformation	4.19E-01; 4.19E-01	WT-1
Renal Hyperplasia / Hyperproliferation	4.51E-01; 4.51E-01	WT-1, GDNF
Renal Dysplasia	6.68E-01; 6.68E-01	H19

Antioxidants and Redox Signaling

The anti-oxidative role of cytoglobin in podocytes: implications for a role in chronic kidney disease. (DOI: 10.1089/ars.2019.7868)

This paper has been peer-reviewed and accepted for publication, but has yet to undergo copyediting and proof correction. The final published version may differ from this proof.

Supplementary Table 6. Differentially expressed genes associated with oxidative stress and apoptosis in shCTGB vs shCTR.

Oxidative stress Gene ID	Fold change	FDR-corrected p-value	Apoptosis Gene ID	Fold change	FDR-corrected p-value
CAT	-1.58	7.28E-06	BCL2L11	-1.47	3.62E-04
CYGB	-28.92	1.10E-98	BID	1.52	2.74E-05
DHCR24	1.87	3.06E-12	BIRC3 (c-IAP1)	-1.57	8.81E-04
DUOX1	-18.36	2.20E-05	BIRC5	-3.83	1.25E-32
DUOX2	-12.61	3.09E-07	CASP1 (ICE)	-1.80	2.77E-04
FOXM1	-2.34	0.00E+00	CASP10 (MCH4)	-1.78	4.27E-07
GCLC	1.51	5.14E-05	CASP3	1.51	2.84E-05
GPX3	-4.69	9.97E-19	CD40 (TNFRSF5)	-1.52	1.00E-02
GPX7	-2.89	1.00E-02	DAPK1	1.62	2.27E-08
NCF2	3.29	3.63E-37	FAS (TNFRSF6)	-1.53	1.21E-06
NUDT1	-1.62	5.04E-06	PYCARD	-2.73	2.72E-06
PRDX2	-1.81	3.82E-14	(TMS1/ASC)	-2.02	0.00E+00
PREX1	-4.71	8.03E-08	TNFRSF11B	3.03	2.31E-24
PTGS1 (COX1)	-2.44	3.33E-04	TNFRSF9	-2.45	2.05E-08
PTGS2 (COX2)	-1.66	3.00E-02	TP73		
SOD3	-3.70	8.01E-04			
UCP2	-1.91	1.14E-09			